

# The rules of human T cell fate *in vivo*

Pedro Costa del Amo<sup>1</sup>, Bisrat Debebe<sup>1</sup>, Milad Razavi Mohseni<sup>2</sup>, Shinji Nakaoka<sup>3,4</sup>, Andrew Worth<sup>5</sup>, Diana Wallace<sup>6</sup>, Peter Beverley<sup>7</sup>, Derek Macallan<sup>8</sup>, Becca Asquith<sup>1</sup>

<sup>1</sup>Department of Infectious Disease, Imperial College London, UK.

<sup>2</sup>Biomedical Engineering Department, Johns Hopkins University, USA.

<sup>3</sup>PRESTO, Japan Science and Technology Agency, Kawaguchi, Japan.

<sup>4</sup>Faculty of Advanced Life Science, Hokkaido University, Japan.

<sup>5</sup>The Jenner Institute Laboratories, University of Oxford, Oxford, UK.

<sup>6</sup>Division of Infection and Immunity, University College London, UK.

<sup>7</sup>TB Research Centre, National Heart and Lung Research Institute, Imperial College London, UK.

<sup>8</sup>Institute for Infection and Immunity, St. George's Hospital, University of London, UK.

**Corresponding author:** Becca Asquith, Dept of Infectious Disease, Imperial College London. +44 (0) 207 594 3731 b.asquith@imperial.ac.uk

**Running title:** The rules of human T cell fate *in vivo*

**Keywords:** lymphocyte, fate, decision, proliferation, lifespan, mathematical model, labelling, half-life

**Abstract length:** 228 words

**Manuscript length:** 7,900 words

**Figures & tables:** 8

## Abstract

The processes governing lymphocyte fate (division, differentiation and death), are typically assumed to be independent of cell age. This assumption has been challenged by a series of elegant studies which clearly show that, for murine cells *in vitro*, lymphocyte fate is age-dependent and that younger cells (i.e. cells which have recently divided) are less likely to divide or die. Here we investigate whether the same rules determine human T cell fate *in vivo*. We combined data from *in vivo* stable isotope labelling in healthy humans with stochastic, agent-based mathematical modelling. We show firstly that the choice of model paradigm has a large impact on parameter estimates obtained using stable isotope labelling i.e. different models fitted to the same data can yield very different estimates of T cell lifespan. Secondly, we found no evidence in humans *in vivo* to support the model in which younger T cells are less likely to divide or die. This age-dependent model never provided the best description of isotope labelling; this was true for naïve and memory, CD4<sup>+</sup> and CD8<sup>+</sup> T cells. Furthermore, this age-dependent model also failed to predict an independent data set in which the link between division and death was explored using Annexin V and deuterated glucose. In contrast, the age-independent model provided the best description of both naïve and memory T cell dynamics and was also able to predict the independent dataset.

## Introduction

The relationship between cell division, differentiation and death is key to many processes in adaptive immunity. Nowhere is this more fundamental to the immune response than in the case of lymphocyte populations, which mount rapid, dramatic expansions and contractions following pathogen challenge; generating both short-lived effectors and long-term memory populations, within the overall context of decades-long lymphocyte homeostasis. Mathematical models of lymphocyte dynamics typically assume that the processes that determine a lymphocyte's fate (division, differentiation, death) are stochastic and independent of the cell's age [1-7]; where cell age is defined as the time since the cell arose from mitosis (**Box 1**). That is, the instantaneous probability of an event is constant and independent of age, hence the probability of a cell dying in the next hour is the same for a "newborn" cell as it is for a 20 year-old cell (provided they are drawn from the same population). Recently, the validity of the age-independent model has been challenged. In a series of elegant studies from the Hodgkin group [8-10], both population level and single cell analysis were used to investigate the interplay between lymphocyte fates. This was formulated into a conceptual age-dependent framework known as the "cyton" model [11]. The central rules of the cyton model are that independent stochastic machinery governs cell processes (e.g. division, differentiation, death), that these processes are competitive and that this machinery is reset upon cell division with (to first approximation) no inheritance of lifespan. Thus if a cell reaches its given time to divide before it reaches its time to die, its progeny will be preserved and indeed expand, whereas, if the converse applies, the cell's progeny will not survive. It is argued that variance in the timing of these events underlies essential features of the adaptive immune response such as rapid expansion or the decision between tolerance and activation. The cyton model has a number of distinct features. In particular cells have an intrinsic "age" which is reset on division; cells that have recently divided are therefore "younger" and have longer to live on average than cells which have not divided recently.

An alternative age-dependent framework, which we refer to as the "risk" model, has also been considered in the literature [12]. According to the risk model, cells which have recently divided are more, not less, likely to die [13]. For T lymphocytes the link between cell activation and cell death, activation-induced cell death, is well-recognised, but its contribution to steady state lymphocyte homeostasis is less clear [14].

Which of these three paradigms (age-independent, cyton or risk) best describes lymphocyte fate is unknown. Age-independence, embodied in the exponential distribution (**Supplementary Fig. S1**), is frequently assumed. At least part of its popularity is due to mathematical convenience: it is a minimal assumption model in which cellular behaviour can be described by a single parameter represented as a rate in ordinary differential equations. However, its popularity is not just attributable to mathematical convenience, there is also a large body of data consistent with exponential survival or growth. Labelled lymphocytes in mice and humans disappear with an apparently constant probability *in vivo* [3, 15-17] and CD4<sup>+</sup> T cell reconstitution following highly active antiretroviral therapy in HIV-1 infection appears to be exponential [18, 19]. However, the age-independent model fails to explain a number of *in vitro* observations. Firstly, close examination of the time-to-die of naïve B cells shows an initial lag followed by an increasing rate of death, consistent with an age-dependent probability of dying. When IL-4 is added, the time to die of the entire population shifts; consistent with a change in the mean of a lognormally distributed time to die rather than a change in the mean of exponentially

distributed times to die [10]. Secondly, the addition of anti-CD3 to naïve CD4<sup>+</sup> T cells shifts the time at which the cells enter their first division, consistent with a lognormally distributed time to first division [20]. Thirdly, there is evidence for competition between cell death and cell proliferation as stimulation of naïve B cells with anti-CD40 and IL-4 had no impact on the loss rate of cells until the time at which surviving cells started to divide [10, 20]. The same pattern has been reported for T cells stimulated with  $\alpha$ CD3 [20]; again this is not consistent with constant probabilities of proliferation and death. Finally, the cyton model produced good fits to both population level and single cell data from CFSE-stained, stimulated B and T cells [10, 11, 21].

These *in vitro* observations support an age-dependent cyton model in which recently divided cells have a reduced risk of death. Furthermore, the authors argue that the cyton model cannot be ruled out by the observation of exponential growth and survival curves since, for certain parameter combinations, age-dependent lognormally distributed times-to-proliferate and times-to-die generate growth and survival curves that are practically indistinguishable from exponential for most experimental set ups [22]. The authors even describe parameter combinations for a single lognormal such that the resulting survival curve appeared biphasic – a common property of many data sets, typically taken as evidence for multiple (age-independent) subpopulations with different kinetic behaviour [7, 12, 23]. Consequently, appearance of exponential survival or growth is not sufficient evidence to rule out age-dependent processes. Hodgkin *et al* have recently extended the cyton model by identifying the mechanism that controls the duration of the clonal burst undergone by B and T cells *in vitro* upon stimulation [24, 25]. In the original version of the cyton model the duration of the proliferative burst (but not the proliferation rate) was inherited between generations but the underlying mechanism was unknown. Analysis of T and B lymphocytes post-stimulation under different conditions revealed that Myc expression levels were approximately the same in all cells upon the termination of the clonal burst, suggesting that Myc levels need to surpass a certain threshold for cell division to occur. Myc expression rates and consequently the duration of the proliferative burst (but again not the proliferation rates) were shown to be inherited with each division. This work supports and extends the cyton model.

In short, there is very good evidence to support the age-dependent cyton model of cell fate for both B and T lymphocytes. However, in order to have a system that can be finely manipulated and readily observed, work to date supporting the cyton model has been conducted almost entirely in murine cells *in vitro*. The one exception which we are aware of is an *in vivo* analysis of T cells in LCMV-infected mice (Supplementary Information in [10]). However, in this work only bulk cell populations were studied, the analysis was restricted to mice and competing models were not considered. It therefore remains an open question whether the cyton model, risk model or age-independent model governs lymphocyte fate in humans *in vivo*.

Which model determines lymphocyte fate *in vivo* is a fundamental question with a number of consequences. Firstly, the assumption that lymphocytes are “age-less” underpins the interpretation of many experiments including labelling with stable isotopes, CFSE and BrdU as well as *in vivo* killing assays [4, 26-28]. Changing this assumption could affect both the dynamic parameters estimated as well as the biological interpretation of the results [29]. Given the ubiquitous application of these techniques (including the study of T cell depletion in HIV-1-infected individuals, T regulatory cell lifespan, T cell origin, cell dynamics in leukemia and diabetes) changes to their interpretation could

have widespread impact [30]. Secondly, immunity is a dynamic process. Understanding how lymphocytes quantitatively regulate their decision-making processes is essential for understanding basic lymphocyte biology.

Here we investigate the rules determining the fate of T lymphocytes in humans *in vivo* during healthy homeostasis. We consider CD4<sup>+</sup> and CD8<sup>+</sup> naïve and memory T cells and focus on two fates: death and division. Our approach is to combine stable isotope labelling *in vivo* (both with heavy water and deuterated glucose), Annexin V staining *ex vivo* and mathematical modelling. We aim to determine: (i) whether the choice of model makes a significant difference to estimates of parameters describing lymphocyte kinetics, (ii) which model best describes heavy water labelling patterns in naïve and memory T cells, and (iii) which model best predicts a new dataset which quantifies the relationship between short-term *in vivo* labelling with deuterated glucose and Annexin V binding as an indicator of incipient death. In this way we set out to elucidate the patterns of division and death which underlie normal lymphocyte behaviour *in vivo*.

## Results

### Impact of model paradigm on estimates of lymphocyte kinetics *in vivo*.

Stable isotope labelling is an established technique for quantifying cell dynamics [5, 31, 32]. Briefly, subjects are given deuterium in the form of deuterated glucose or heavy water. Deuterium is incorporated into the DNA of cells when they divide and lost when labelled cells die or differentiate. Cells of interest are sampled and the level of deuterium incorporated into their DNA is quantified by mass spectrometry. The rate of cell proliferation and the rate of cell disappearance are estimated by fitting a mathematical model to the labelling data and finding the values of the rates which minimise the discrepancy between data and prediction. The mathematical models used to interpret stable isotope labelling data typically assume that cells proliferate and die/differentiate in an age-independent manner [3, 5, 7, 23, 33-38]. To investigate the extent to which estimates of proliferation would change if the age-independent assumption was relaxed, we developed an agent-based model (ABM) of a population of cells in homeostasis (Methods). The ABM simulated the labelling and delabelling phases of a deuterium labelling experiment, modelling division and disappearance events according to each of the paradigms of cell fate. In the ABM, cells were initialized upon birth (mitosis) with times to divide and to disappear drawn from a gamma or lognormal distribution. We investigated three paradigms:

- i. the cyton model, in which the probability of a cell dying or dividing increases with its age;
- ii. the risk model, in which the probability of death or division decrease as the cell ages;
- iii. the age-independent model, in which the probability of death or division is independent of age.

The parameters of the distribution determine which paradigm the simulated population obeys (**Supplementary Fig. S1**). When the distribution is exponential (gamma with rate=1) then the probability of an event (conditioned on survival to that point) is independent of age and the age-independent model is captured. When the distribution is gamma with shape parameter lower than one then the distribution of time to an event has a zero mode and a steeper slope than the exponential distribution and the probability of an event decreases with age, i.e. the risk paradigm is captured. When the distribution is gamma with a shape parameter higher than one then the mode is greater than zero, probability of an event increases with age and the cyton paradigm is captured. For the lognormal distribution, the mapping between the parameters and paradigms is less precise but when the location parameter is large relative to the scale then the distribution is strongly right-skewed and the mode is much greater than zero (cells much less likely to die or divide immediately after a previous division event) and the cell behaviour conforms to the cyton paradigm; as the location parameter decreases relative to the scale then the mode decreases and the behaviour becomes risk-like. We reiterate that we define the age of a cell as the time since creation of the cell by mitosis (**Box 1**).

We considered both a homogeneous cell population and a heterogeneous population consisting of two subpopulations. Under the heterogeneous scenario, both subpopulations were governed by the same form of distribution (i.e. two exponentials, two gammas or two lognormals) with varying parameters. We thus had 6 models (**Table 1**): two (Model 1 and 2) were age-independent, the remaining four were age-dependent models with Models 3 and 4 obeying the cyton paradigm and models 5 and 6 the risk paradigm. For the cyton and risk models we considered the populations to be governed either by gamma or lognormal distributions; for brevity we focus on results from the gamma

distribution in the text; results obtained with the lognormal distribution are similar unless stated otherwise and are presented in the figures and supplementary information.

These models, representing the three paradigms, were fitted to experimental data from a published stable isotope-labelling study [33]. In this study, 5 healthy human volunteers were given heavy water ( $^2\text{H}_2\text{O}$ ) for 63 days and the fraction of label incorporated in the DNA of naïve ( $\text{CD}27^+\text{CD}45\text{RO}^-$ ) and memory ( $\text{CD}45\text{RO}^+$ )  $\text{CD}4^+$  and  $\text{CD}8^+$  T cells was measured at successive time points.

**Naïve  $\text{CD}4^+$  and  $\text{CD}8^+$  T cells.** We found that the homogeneous population models consistently provided a better description of the naïve cell labelling data than heterogeneous population models, in agreement with the literature [7, 12]. So, when considering the impact of model choice on parameter estimates, we restrict ourselves to the homogeneous versions of the three paradigms (age-independent, cyton and risk). The median lifespan (time to death or division) estimated from the three models are shown in **Fig.1**; the distribution of lifespans are shown in **Supplementary Fig. S2**. The age-dependent cyton model gave the longest estimates of naïve cell lifespans; they were systematically greater than lifespans obtained using the age-independent model ( $P=0.002$ , mean difference=366 days, 49% increase, Wilcoxon signed rank two-tailed) and even longer than lifespans obtained using the risk model ( $P=0.002$ , mean difference=465 days, 72% increase). The lognormal version of the cyton model gave similar results to the version based on the gamma distribution described above whilst the lognormal version of the risk model failed to fit the experimental data.

**Memory  $\text{CD}4^+$  and  $\text{CD}8^+$  T cells.** Previous studies assuming age-independent models of lymphocyte dynamics have suggested that memory cell pools are kinetically heterogeneous - at least two exponentials being required to capture their dynamics [7, 39, 40]. However, Dowling et al. [22] have shown that, for certain parameter combinations, the lognormal distribution results in biphasic survival curves which could be mistaken for the signature of a heterogeneous population, when age-dependence is not taken into account. Therefore, we do not make any assumption about whether the memory T cell populations are kinetically homogeneous or heterogeneous.

The estimated median lifespans are presented in **Fig. 1**, the lifespan distributions are given in **Supplementary Fig. S3**. In all cases the heterogeneous version of a model yielded longer lifespans than the corresponding homogeneous version ( $P=2 \times 10^{-9}$ , mean difference=212 days, 105% increase). Within both the homogeneous and heterogeneous models we saw the same ranking of lifespans as for naïve cells i.e. the cyton model gave the longest lifespans, followed by the age-independent model with the risk model giving the shortest lifespans. If the cyton model described by the lognormal distribution is mistakenly identified as heterogeneous age-independent, as suggested [22], then this would result in a significant overestimate of median lifespan ( $P=0.002$ , mean difference in lifespan homogeneous cyton v heterogeneous age-independent = 298 days, 360% increase).

We conclude that assumptions about the underlying paradigm can have considerable impact on estimates of lymphocyte lifespan calculated from stable isotope labelling data.

## Which paradigm provides the best description of stable isotope labelling data?

**Naïve CD4<sup>+</sup> and CD8<sup>+</sup> T cells.** In order to determine which paradigm provides the best description of T cell fate we fitted the different models to the stable isotope labelling data described above and compared the quality of the fit using the Corrected Akaike Information Criterion (AICc [41], Methods). For naïve CD4<sup>+</sup> and CD8<sup>+</sup> T cells, the homogeneous age-independent model provided a better description of the experimental data than either the homogeneous cyton or the homogeneous risk models in 10/10 cases (**Fig. 2**, AICc for the age-independent model significantly lower than the best fitting age-dependent model  $P=0.002$ , two tailed Wilcoxon, lower AICc indicating a better description) but the median difference in AICc was small (2.7). The heterogeneous cyton and risk models were not competitive (lose in 10/10 cases,  $P=0.002$ ) and the median difference in AICcs was large (19.5). The heterogeneous models failed because they have a larger number of parameters but do not offer a better fit than the homogeneous models (**Supplementary Fig. S4, Supplementary Table S1**). In summary, for naïve CD4<sup>+</sup> and CD8<sup>+</sup> T cells, the data (i) support a homogeneous model rather than a heterogeneous model and (ii) provide no evidence to support age-dependence.

**Memory CD4<sup>+</sup> and CD8<sup>+</sup> T cells.** Despite the fact that we considered 4 times more age-dependent than age-independent models (risk and cyton; lognormal and gamma formulations) the age-independent models provided the best description of the memory T cell data in 7/10 cases. Where data was dense the heterogeneous version of the age-independent model was successful (5/10 cases); where data was limited the homogeneous age-independent model was preferred (**Fig. 2**). The homogeneous risk model (lognormal distribution) was better in the remaining three cases, but by small differences in the AICc (mean 2.1, **Supplementary Table S2**). The cyton model (in either heterogeneous or homogeneous form) was never competitive; losing in 10/10 cases (mean difference in AICc between cyton and winning model: 22.1). The plots of the fits for Memory CD4<sup>+</sup> and CD8<sup>+</sup> T cells are shown in **Fig. 3**. In summary, the dynamics of CD4<sup>+</sup> and CD8<sup>+</sup> T cell memory cells *in vivo* are best described by age-independent models; the cyton model performs poorly.

**Approach validation.** It is noticeable that, when comparing the fit of the different paradigms to the experimental data, many models produce a similar fit and that the age-independent model therefore tends to win because it has fewer parameters. We were concerned that this approach may be biased against the more complicated models because the data may not be sufficiently dense to identify the age-dependent models. We therefore investigated whether age-dependent models, if they were true, would be expected to generate sufficient signal in these types of data sets to be identified. We generated *in silico* datasets of different sizes (with noise) consistent with a known paradigm and then investigated if our approach could correctly identify the generating paradigm (**Methods**). We found that when the generating model was the cyton model (either lognormal or gamma) the generating model was always correctly identified and (with the exception of one model for the smallest dataset  $n=6$ ) no other model came within 6 AICc of the generating model (**Fig. 4A**). When the generating model was risk, for the lognormal version the generating model was always correctly identified; for the gamma version the generating model was correctly identified the majority of the time and when it was not the winning model it was always within 1 AICc of the winning model i.e. it was indistinguishable from the winning model (**Fig. 4B**). When the generating model was the age-independent heterogeneous model then the winning model was the generating model for  $n \geq 11$ , though for  $n=11$  (but not higher) other models were competitive. For the age-independent

homogeneous model then the winning model was, unexpectedly, gamma risk and this did not improve even for very large data sets (**Fig. 4C**). On investigating this further, we found that the winning version of the gamma risk model always had shape parameter close to 1 (mean 0.97) i.e. the winning model was very close to the age-independent exponential but the additional freedom to slightly decrease the shape parameter resulted in an improved fit. Of note, there was never a case when data generated by any age-dependent paradigm was misclassified as age-independent. In summary, the approach performs well but has a slight bias against the age-independent model; it robustly identified the cyton model whenever it was the generating model. We conclude that the age-dependent models should be distinguishable from age-independent models with this type and density of data and that it is unlikely that cell dynamics consistent with the cyton model would be misidentified as coming from an age-independent model.

**Alternative approach.** We have shown that fitting the models to the experimental data and comparing their AICCs provides support for the age-independent family of models. Furthermore, *in silico* testing indicated that this approach performs well. Nevertheless, we were still concerned that this approach suffers from a dependence on the number of data points relative to model complexity; we therefore implemented an alternative method. In the previous approach (above) we compared models on the basis of their AICCs by restricting parameter ranges such that the distributions obeyed either the age-independent, risk or the cyton paradigm. For the alternative approach, we took advantage of the fact that a single gamma distribution can describe all three paradigms. We allowed parameters to vary freely, effectively ranging over all paradigms, and then investigated which paradigm the best fit parameters corresponded to. In this way all models were considered equally without reference to model complexity. We reiterate that, for the gamma distribution a shape parameter less than 1 corresponds to the risk paradigm, a shape parameter equal to 1 corresponds to the age-independent paradigm and a shape parameter greater than 1 corresponds to the cyton paradigm.

For naïve T cells the shape parameter was poorly identifiable; in most cases the CI included 1 (i.e. shape parameter not significantly different from one). For memory T cells the shape parameter could be estimated more accurately and in all cases was very close to one (**Fig. 5**). These results closely mirror those obtained using the AICc. That is, for naïve T cells it is difficult to distinguish between paradigms but there is no clear support for the cyton model. Whilst for memory T cells, the dynamics are best described by the age-independent paradigm.

We wished to extend this alternative approach to investigate the lognormal family of distributions. The problem arises that for the lognormal distribution, unlike the gamma distribution, there are no parameter combinations such that the lognormal distribution is age-independent, nor is there a precise mapping between parameter combinations and the age-dependent paradigms. Instead we looked at the (instantaneous) probability of death conditioned on survival to that point. If the underlying paradigm is risk then we would expect a strong left skewed distribution (i.e. cells more likely to die immediately after division) whereas if the underlying paradigm is cyton-like then the probability of death would increase with time (older cells more likely to die). We found that for naïve T cells the distributions were rather poorly identified. For memory T cells the picture was much clearer, for both a homogenous and a heterogeneous lognormal model the probability distributions were much more consistent with the risk rather than the cyton paradigm (**Supplementary Figure S5**). Age

independent paradigms could not be considered for the lognormal distributions within this framework but it is clear that there is little support for the cyton model.

### **Measurement of deuterated glucose labelling in Annexin V–positive and –negative cells**

A model's ability to predict new data is as important, and arguably a more stringent test, than its ability to fit existing data. We therefore generated an independent dataset consisting of a different type of data against which to assess the models. As we were interested in the temporal link between division and death we combined deuterated glucose pulse-labelling with separation of cells during follow-up according to a marker of incipient apoptosis, Annexin V binding. Annexin V is a protein which binds to phosphatidylserines translocated to the outer membrane during apoptosis; its binding on the cell surface is an early indicator of apoptosis. In this way we explored the relationship between recent division and risk of death.

Four healthy adults received deuterated glucose ([6,6-<sup>2</sup>H<sub>2</sub>]-glucose) as an intravenous infusion for 24h. Blood samples were taken at successive time points post-infusion and CD4<sup>+</sup> memory (CD45RO<sup>+</sup>) T lymphocytes were sorted by flow cytometry into Annexin V-positive and Annexin V-negative subsets and deuterium incorporation into cellular DNA in each subset was quantified (**Fig. 6A**).

### **Prediction of Annexin V labelling signatures**

We wished to ascertain the ratios of Annexin V-positive and -negative cells in labelled and unlabelled cell populations. This cannot be measured directly, i.e. we cannot sort labelled and unlabelled cells and then quantify Annexin V binding, as the measurement of label requires the destruction of the cells (their DNA is isolated and hydrolysed). Instead we calculate the ratio at days 3 and 7 from the proportion of label in the Annexin V-positive and -negative cells (**Methods**). This analysis revealed a distinct signature in the experimental data (**Fig. 6B**): the fraction of Annexin V-binding cells in the labelled population was consistently higher than the fraction in the non-labelled population at both days 3 and 7 ( $P=0.008$ , Wilcoxon two tailed). We investigated the ability of the 6 different models (**Table 1**) to predict this signature.

For each model we took the best fit parameter combinations generated in the previous section by fitting to heavy water labelling of Memory CD4<sup>+</sup> T cells, and then used these parameters to predict the outcome of the Annexin V/deuterated glucose experiment using the ABM. Apoptosis has been shown to last for 12-24 hours [42], and the translocation of phosphatidylserines to the outer part of the membrane of the cell is known to occur from an early stage of the process [43]. Accordingly, we approximated the fraction of Annexin V-binding cells in labelled and non-labelled cell populations by the fraction of simulated cells with remaining lifetimes lower than 24 hours. We then investigated the models' ability to predict the observed signatures. The fraction of Annexin V-binding cells *ex vivo* is known to overestimate the fraction of cells dying *in vivo* by at least 50-fold [33, 44] (presumably because not all Annexin V-binding cells die [45, 46] and because taking cells *ex vivo* increases death [47]); furthermore the individual subjects being simulated are different from the individuals subjects fitted so we did not aim to predict the absolute levels of label incorporation (which shows considerable inter-individual variation). Instead we aimed to predict the observed signature which was clear and consistent across all four individuals (**Fig. 6B**).

Of the six models considered, three successfully predicted the observed signature. The heterogeneous age-independent, and both the homogeneous and heterogeneous risk models correctly predicted that the fraction of Annexin V+ cells was significantly higher amongst labelled cells than non-labelled cells at day 3 and at day 7 (**Fig. 6C**). Intuitively, this makes sense: if the population is heterogeneous age-independent then the subpopulation with faster kinetics will be overrepresented amongst the labelled cells. These cells die faster than the slow population labelled cells and thus will express a higher proportion of Annexin V. Similarly, under the risk paradigm, recently divided (i.e. labelled) cells will have a greater risk of dying. The homogeneous age-independent model and both homogeneous and heterogeneous versions of the cyton model failed to predict the signature and were not consistent with the experimental observations (**Fig. 6C**).

## Discussion

T cell proliferation and death are typically assumed to be independent of cell age (where age is defined as time since division). However, it has been postulated that lymphocyte division and death are governed by the age-dependent cyton model and that this form of immune regulation permits rapid induction of a wide range of responses from tolerance to strong immunity on the basis of small changes in mean time to divide, die or differentiate [10, 20]. There is very strong evidence that murine lymphocytes *in vitro* obey the cyton model [10, 11, 20, 21, 48]. To investigate whether T lymphocytes in humans *in vivo* also obey this age-dependent model, we combined mathematical modelling, analysis of existing heavy water labelling data and generation of new Annexin V and deuterated glucose labelling data.

Our main conclusions are that firstly, the choice of model paradigm has a large impact on estimates of cell lifespan obtained using stable isotope labelling. It seems likely that this conclusion will also apply to the interpretation of CFSE and BrdU labelling data. Secondly, we found no evidence to support the cyton model as a description of T cell dynamics in humans *in vivo*. No version of the cyton model (neither homogeneous nor heterogeneous, lognormal nor gamma) ever provided the best description of *in vivo* heavy water labelling. This was true for all four T cell populations considered: naïve CD4<sup>+</sup> T cells, naïve CD8<sup>+</sup> T cells, memory CD4<sup>+</sup> T cells and memory CD8<sup>+</sup> T cells. An alternative approach which was independent of model complexity (fitting an unconstrained gamma or lognormal distribution) also found no evidence for the cyton model. Furthermore, the cyton model (all versions) also failed to predict patterns in an independent, newly generated data set. Thirdly, the age-independent exponential model provided the best description of both naïve and memory T cell dynamics. Age-independent models provided the best fit to naïve T cell labelling data in 10/10 cases and to memory T cell labelling data in 7/10 cases, though differences were not always large. The age-independent model was also able to predict the novel Annexin V dataset. Our finding in favour of an age-independent paradigm is not inconsistent with the Hayflick limit. Age as defined by telomere shortening is counted from haematopoiesis and is distinct from, and on a different timescale to, the age since division which we focus on. Additionally, the action of telomerase, which is up-regulated in dividing lymphocytes [49], may mean that most T cell death is independent of the Hayflick limit. Time since haematopoiesis will be related to the age of the individual subject, the association between age of the individual and T cell dynamics has recently been studied in mice [50].

Given that the evidence for the cyton model *in vitro* is so strong, it is surprising that it fails to explain lymphocyte dynamics *in vivo*. There are at least three possible explanations. Firstly, the difference may relate to the difference between conditions *in vitro* and *in vivo*. *In vivo*, even if a cell's intrinsic programme is age-dependent, randomly encountered cell-exogenous stimuli such as cytokines, cell-cell contact or antigen may render its resultant behaviour age-independent. That is, lymphocytes may have an age but other factors dominate *in vivo* so in practice age does not determine their fate [51]. Of note, in many of the *in vitro* experiments supporting the cyton model, autocrine IL-2 is blocked [20, 48, 52]. Specifically, in cultures of murine T cells, murine IL-2 (mIL-2) is blocked by the addition of an antibody and then the media supplemented with a fixed concentration of human IL-2 which is active on murine T cells but not blocked by the mIL-2-specific antibody. In this way the natural effect of autocrine IL-2 is removed. This is one example of a possible stimuli that would be present *in vivo* but has been excluded *in vitro* and which could have a profound effect on T cell behaviour. Secondly, the

difference may relate to differences between mice and humans. Human and murine immune systems face different selection pressures and may have evolved different behaviour. For instance, there is evidence that the lifespan of memory and naïve T cells and the maintenance of naïve T cell homeostasis are very different in humans and mice [15]. However, a study by Gossel *et al* [40] which studied the dynamics of memory CD4<sup>+</sup> T cells in mice *in vivo*, also found that Ki67<sup>+</sup> (“young”) cells had lifespans that were indistinguishable from Ki67<sup>-</sup> (“old”) cells providing strong support for an age-independent model compared to age-independent alternatives in mice *in vivo*. This agrees well with our conclusions in humans, suggesting that the difference is more likely to relate to *in vitro* v *in vivo* conditions rather than mice v humans. Finally, the difference may relate to differences in stimulation. In the scenarios we modelled there was no overt infection, whilst in the work supporting the cyton model, lymphocytes were always stimulated exogenously. Since the individuals we studied did not have any symptomatic infection we did not simulate the “division destiny” of lymphocytes (duration of the division burst of B and T cells after stimulated *in vitro*) which is a feature of the cyton model [10, 24]. It would be interesting to repeat our work in individuals with ongoing infection to see if the rules of cell fate were altered. Nevertheless, the authors of the cyton work have always argued that the cyton paradigm also explains lymphocytes in homeostasis [10] and have investigated the consequences of the cyton paradigm in homeostasis upon thymus involution and aging [53, 54].

A potential concern about our approach is the use of the AICc for comparing models. Although such an approach is an appropriate, accepted technique [41] and is widely used for model selection e.g.[55, 56] it does identify the minimal model needed to describe the data rather than the “true” model. For naïve T cells, all the models fitted the data in a very similar way and so the winning model is necessarily the model with the least number of parameters i.e. the age-independent homogeneous model. For this reason our conclusion for the naïve cells is simply that there is no evidence to support age-dependence. However, for memory T cells, age-independent models consistently out-perform age-dependent models despite not having consistent differences in complexity. The winning model in most cases (age-independent heterogeneous) is more complicated than the cyton model (3 parameters for age-independent compared with 2 for cyton). When data becomes sparse (some people missed some sampling time points) and there is insufficient data to support the heterogeneous age-independent model, the winning model jumps to the homogeneous age-independent model (1 parameter) rather than any of the age-dependent options which have intermediate complexity. These conclusions were supported by a number of additional pieces of work. Firstly, *in silico* simulations suggests that our approach is unlikely to incorrectly favour an age-independent model if the generating model is actually the cyton model; if anything the approach is biased against age-independence. Secondly, when using a model with the same number of parameters for the age-independent, cyton and risk model (i.e. gamma distribution with unconstrained parameters) then for memory cells the age-independent model was strongly favoured. Finally, our conclusions are supported by predictions of a new independent data set.

All the models considered contain a number of simplifying assumptions. This is essential to avoid over parameterisation but has the potential to affect our results. Firstly, we assume that there is no inheritance of times to die or to divide between subsequent generations of cells. To a first approximation this is true; even in the earlier studies of cell fate where detailed *in vitro* measurements were made there was no evidence to support inheritance [10, 20, 22, 57]. However, very fine single cell fate mapping has revealed signals for complex inheritance between cousins [21]. Secondly, we

neglect cell flow into the cell populations. We have shown in humans [35] and others have shown in mice [40] that such constitutive flow is ongoing even in homeostasis. Finally, we have assumed that both death and division of a given population can be described by the same probability density function (same parameters). The impact of these various assumptions cannot be directly explored due to the number of additional, correlated parameters which would need to be introduced. For instance, to investigate the third point above, we relaxed the assumption that death and division were described by the same distribution and considered two additional homogeneous age-dependent models of cell fate, in which division and death mechanisms were expressed by different probability density functions of the same form (gamma or lognormal). These models never outperformed the other versions in any of the cases but this is most likely due to the excess complexity of the new models (i.e. the data are not sufficiently rich to support the more complex models). Although it is not possible to explicitly analyse these simplifying assumptions we note that they have been applied to all paradigms equally. All participants were aged under 50 years. We therefore cannot know whether the rules of cell fate in the elderly are best described by a cell age-dependent or cell age-independent model.

In general, the work that can be performed in humans is very limited compared to what can be achieved with murine cells *in vitro*. We are restricted to studying population averages rather than single cells and must rely on natural physiology rather than use knockouts or transfectants. Nevertheless, the different paradigms do predict distinct patterns of behaviour that can be detected at the cell population level in the absence of manipulation enabling us to distinguish between them. In summary, the cyton model provides a compelling hypothesis to explain how the immune system interleaves lymphocyte fate to achieve a robust, diverse response; it is strongly supported by *in vitro* work using murine cells. Unexpectedly, using three different approaches, we find no evidence that it describes T cell fate in healthy humans *in vivo*. Additionally, we show that extreme care needs to be taken in selecting models for estimating lymphocyte dynamic parameters as the choice of the underlying paradigm can have a profound impact on the estimates derived. Given the strength of the evidence for the cyton model *in vitro* we suggest that age probably determines cell fate *in vitro* but *in vivo*, where cells receive a huge number of external stimuli from other cells, antigen and cytokines, extrinsic factors rather than age are more likely to determine cell fate. A useful analogy is human lifespan. Fundamentally, the time when a human dies depends on their age and, in the developed world in peacetime, this pattern is manifest and age is a major determinant of the probability of death. However, during wartime, death is largely a random event and time of death is independent of a person's age. We suggest that the cyton model describes the fundamental rule of cell fate and is manifest "in peacetime" (*in vitro*) but in war (*in vivo*) these effects are overridden.

The age-independent exponential distribution is usually assumed but rarely justified. Here, we show that, *in vivo* for memory and naïve CD4<sup>+</sup> and CD8<sup>+</sup> T cells in healthy humans, the age-independent model appears to provide the best description of cell fate in homeostasis.

## Materials and Methods

### Ethics statement.

All subjects gave written informed consent following Ethical Review Board approval (Ref 10/H0803/102 and 13/LO/0022); all interventions were performed according to the principles of the Declaration of Helsinki.

### Agent-based model.

We developed an agent-based model (ABM) to simulate stable isotope labelling of a population of cells in homeostasis. Upon birth (by division of the mother cell), cells were assigned times to die/differentiate and to divide which were drawn from a defined distribution (gamma or lognormal). The time step in the model is 1 day. After each time step, the age of the cell is increased by one day. If the age becomes equal to the time to die/differentiate, the cell is removed from the population. If it reaches its time to divide, it is substituted by two new daughter cells of age 0 with times to die/differentiate and to divide which are drawn again from the defined distribution. The model was implemented in C++.

**Kinetic heterogeneity.** We allow for both kinetically homogeneous and heterogeneous populations. In a heterogeneous configuration, each subpopulation is assigned a different distribution of times to die/differentiate and times to divide. For a population consisting of  $n$  subpopulations,  $n-1$  ratios are required to specify the proportions at which each of them is found. Each subpopulation is assumed to be independently in homeostasis, and the progeny of a given cell belong to the same subpopulation as the mother cell (i.e. its times to an event are drawn from the same distribution).

**Deuterium labelling process.** We simulate both heavy water and deuterated glucose labelling experiments. During the labelling period  $\tau$ , each time that a cell divides, it is replaced by two daughter cells that are labelled in proportion to the label availability. In the case of heavy water, the availability of label is described by the following empirical equation [33]:

$$\begin{aligned} U(t) &= f(1 - e^{-\delta t}) - \beta e^{-\delta t} && \text{during label intake } t \leq \tau \\ U(t) &= [f(1 - e^{-\delta \tau}) - \beta e^{-\delta \tau}] e^{-\delta(t-\tau)} && \text{after label intake } t > \tau \end{aligned}$$

In the case of deuterated glucose, because of the fast turnover rate of glucose, availability of label is assumed to follow a square pulse [17]:

$$\begin{aligned} U(t) &= U && \text{during label intake } t \leq \tau \\ U(t) &= 0 && \text{after label intake } t > \tau \end{aligned}$$

The parameters ( $f$ ,  $\delta$ ,  $\beta$ ,  $U$ ) were estimated by fitting to successive measurements of label availability in plasma in the case of deuterated glucose or urine in the case of heavy water (**Supplementary Table S4**).

**Model initialization.** In the ABM the remaining lifetime of the population will evolve in time as the population ages. Since we were studying adults, we assumed the cell population had reached steady state. We therefore initialize the times to die/differentiate and to divide in the ABM, from the steady state distributions of remaining lifetime which we derived analytically (**Supplementary Information**).

**Fitting the model.** The fitting of the ABM to the experimental data with an ordinary least squares objective function was carried out using the global optimisation algorithm pseudoOptim from

the FME package in R [58]. To minimize stochasticity, 5 different random seeds were considered each time a labelling curve was generated in C++ and the median of the 5 costs used. The number of free parameters depended on the model assumed (**Table 1**).

**Age-independent, Cyton and Risk paradigms.** The three paradigms are captured by non-overlapping parameter spaces of the gammas and lognormal distributions of times to die/differentiate and to divide. The parameter ranges of the fitting procedures were configured accordingly for each case. For the gamma distribution, shape parameters equal to one (exponential distribution) are characteristic of an age-independent population; shape parameters lower than one (zero mode) are characteristic of the risk model; and shape parameters higher than one (higher than zero mode) are representative of the cyton model. For the lognormal distribution, we imposed the restriction that distribution modes had to be higher than seven days, or lower than two respectively. The upper bound on the scale of the lognormal was set to 2.5; this was sufficient to observe dramatic risk behaviour. Increasing the scale parameter to a value of 3 improved the fits of the homogeneous age-dependent risk model with one lognormal (not enough to change the results), but resulted in lifetimes which were unrealistic (in many cases, more than 25% of the population died or divided in the first 24h. after division), **Supplementary Table S3**. Extending these limits further resulted in unfeasible fitting times due to the integration routines in the ABM. Additional details regarding the ABM are included in the Supplementary Information. Examples of the relationship between the distributions of time to die/differentiate and divide and the age-dependence of probabilities are provided in **Supplementary Figure S1**.

#### **Corrected Akaike Information Criterion (AICc).**

We use the AICc metric to compare different models [41]. The AICc introduces a penalty for the number of parameters and a correction for small sample size:

$$AICc = n \ln \left[ \frac{ssr}{n} \right] + \frac{2nk}{n - k - 1}$$

where *ssr* is the sum of squared residuals, *k* is the number of estimated parameters and *n* is the number of data points. The best model is identified by the lowest AICc. A frequently used rule of thumb states that an AICc difference < 2 is not sufficient to empirically support the winning model; that a difference of 6 is considered as sufficient; and that a difference >10 favours one model with confidence [59]. The absolute value of the AICc is not meaningful so we report the normalised AICc which is defined as the difference between the AICc and the AICc of the winning model (and is therefore zero for the winning model).

#### **Approach validation**

To investigate whether the approach of fitting the different models to the data and selecting the model with the lowest AICs yielded the correct model (i.e. the model which generated the data) we performed the following study. For each of the six models considered (homogeneous exponential, heterogeneous exponential, homogeneous gamma cyton, homogeneous gamma risk, homogeneous lognormal risk and homogeneous lognormal cyton) we simulated data. Specifically, we first simulated data from the model using realistic parameters (parameters were chosen based on fits to the heavy water data from the previous section), added noise to each data point (random variables sampled from  $N(0, 0.025)$ ) and selected datasets of varying size ( $n=6, n=11, n=20, n=30, n=50$ ). For the  $n=11$

simulated data we chose timepoints which coincided exactly with our experimental time points;  $n=6$  is a subset of these and  $n>11$  an extension of these. We then fitted each of the 6 models to each of these  $5 \times 6=30$  datasets and calculated the AICc. We then analysed whether the winning model (model with the lowest AICc) was the model which was known to generate the data.

### **Alternative approach**

We also developed an approach that did not rely on the AICc and was thus independent of model complexity. Instead of constraining the gamma or lognormal distributions to adopt parameters consistent with a given paradigm and comparing the fits we allowed the distributions to take up any parameter combination, effectively allowing the distributions to vary across the paradigms. For the gamma distribution there is a clear mapping between the parameters of the distribution and the paradigms (shape parameter=1: age-independent distribution, shape parameter<1: risk paradigm, shape parameter>1: cyton paradigm). The lognormal distribution is less useful as it cannot capture the age-independent paradigm and the mapping between parameters and age-dependent paradigms is imprecise. To investigate the best fitting lognormal distributions we plotted the probability of an event conditioned on survival to that point calculated from the best fit distribution (equations given in Supplementary Information). For the risk paradigm the distribution of the conditional probability would be expected to be strongly left-skewed with a decreasing probability with age, for the cyton paradigm there would be more weight to the right with probabilities increasing with age. To illustrate the spread of distributions we also plotted 100 trajectories created by sampling the parameters from the normal distribution centered on the best fit parameter with standard deviation the standard deviation of the parameter estimate.

### **Heavy water data**

Previously published *in vivo* heavy water labeling data from five subjects were re-analyzed using the ABM (above). Experimental details have been published elsewhere [33]. Briefly, healthy young adults (age 20-25) received heavy water for 9 weeks comprising a prime of 10ml  $^2\text{H}_2\text{O}$  /kg body weight over 24h followed by 1.25ml  $^2\text{H}_2\text{O}$  /kg body weight daily. Cell samples were taken at successive time points; urine samples were measured for body water enrichment. Label enrichment in the DNA of Naïve ( $\text{CD45RO}^- \text{CD27}^+$ ) and Memory ( $\text{CD45RO}^+$ ),  $\text{CD4}^+$  and  $\text{CD8}^+$  T cells were measured by GC-MS.

### **Deuterated glucose and Annexin V+ data**

Four healthy adults (independent of the individuals studied by heavy water labelling) were labelled *in vivo* using a previously described protocol [5, 12]. Briefly, all received 6,6- $^2\text{H}_2$ -glucose as a primed, 24-hour intravenous infusion. Cells dividing during the labelling phase become labelled by incorporation of deuterium into their DNA. 50ml of blood was taken at days 3, 4, 7 and 8; PBMC were isolated by Ficoll gradient centrifugation and  $\text{CD3}^+ \text{CD4}^+ \text{CD45RO}^+$  lymphocytes were separated within 4 hours of venepuncture by flow cytometry (Moflo flow cytometer, Cytomation, Fort Collins, CO) according to Annexin V binding into two populations:  $\text{CD4}^+ \text{CD45RO}^+$  Annexin V-bright and  $\text{CD4}^+ \text{CD45RO}^+$  Annexin V-negative T cells; cells expressing intermediate levels of Annexin-staining were not collected in this analysis. Forward / side-scatter gating was used to exclude dead cells and cellular debris. DNA was extracted and hydrolysed to nucleosides and deuterium enrichment in DNA measured by gas-chromatography mass-spectrometry as previously described [1, 5] using the PCI derivative monitoring ions  $m/z$  198 and 200 (Agilent GCMS, Agilent, Bracknell, UK).

The fractions of cells labelled and unlabelled at each time point were quantified for both Annexin V-positive and -negative cell populations for the 4 subjects. The fraction of Annexin V-positive cells amongst labelled and unlabelled cells were derived from those fractions as the ratio of the Annexin V-positive cells and the sum of both Annexin V-positive and -negative populations in labelled and unlabelled groups respectively. This cannot be measured directly i.e. we cannot sort labelled and unlabelled cells and then quantify Annexin V expression as the measurement of label requires the destruction of the cells (their DNA is isolated and hydrolysed).

### **Acknowledgements**

We would like to thank Lies Boelen, Rob de Boer, José Borghans, Julia Drylewicz, and Phil Hodgkin for very helpful discussions on this work and Jonas Mackerodt for help with the model fitting. The research leading to these results has received funding from the European Union Seventh Framework Programme (FP7/2007-2013) under grant agreement 317040 (QuanTI). B.A. is a Wellcome Trust Investigator (103865) and is funded by the Medical Research Council UK (J007439 and G1001052), the European Union Seventh Framework Programme (FP7/2007–2013) under grant agreement 317040 (QuanTI) and Leukemia and Lymphoma Research (15012). DCM received funding from the Medical Research Council UK (G1001052). SN received funding from the JST PRESTO program (JPMJPR16E9) and the Japan Society for the Promotion of Science (JSPS) Grants-in-Aid 25871132 and 16K052565. The Imperial College High Performance Computing Service was used for this work.

### **Contribution statement**

PCdA designed research, performed research analyzed data, and wrote the paper. BD contributed vital new computational tools, and analyzed data. MRM performed research. SN contributed vital new computational tools. AW, DW and PB performed research. DM performed research and wrote the paper. BA designed research, performed research, analyzed data, and wrote the paper.

### **Conflict of interest statement**

None of the authors has a relevant conflict of interest.

## References

1. McLean AR, Michie CA. In vivo estimates of division and death rates of human T lymphocytes. *Proc Natl Acad Sci U S A*. 1995;92(9):3707-11. PubMed PMID: 7731969.
2. Ramalho, Curado, Natarajan. Lifespan of human lymphocytes estimated during a six year cytogenetic follow-up of individuals accidentally exposed in the 1987 radiological accident in Brazil. *Mutat Res*. 1995;331:47-54.
3. Asquith B, Zhang Y, Mosley AJ, de Lara CM, Wallace DL, Worth A, et al. In vivo T lymphocyte dynamics in humans and the impact of human T-lymphotropic virus 1 infection. *Proc Natl Acad Sci U S A*. 2007;104(19):8035-40. doi: 10.1073/pnas.0608832104. PubMed PMID: 17483473; PubMed Central PMCID: PMC1861853.
4. Slifka MK, Antia R, Whitmire JK, Ahmed R. Humoral immunity due to long-lived plasma cells. *Immunity* 1998;8:363-72.
5. Macallan DC, Asquith B, Zhang Y, de Lara C, Ghattas H, Defoiche J, et al. Measurement of proliferation and disappearance of rapid turnover cell populations in human studies using deuterium-labeled glucose. *Nat Protoc*. 2009;4(9):1313-27. doi: 10.1038/nprot.2009.117. PubMed PMID: 19696750.
6. Tanchot C, Rocha B. The organization of mature T-cell pools. *Immunol Today*. 1998;19(12):575-9. PubMed PMID: 9864949.
7. Westera L, Drylewicz J, den Braber I, Mugwagwa T, van der Maas I, Kwast L, et al. Closing the gap between T-cell life span estimates from stable isotope-labeling studies in mice and humans. *Blood*. 2013;122(13):2205-12. doi: 10.1182/blood-2013-03-488411. PubMed PMID: WOS:000325269900012.
8. Gett AV, Hodgkin PD. Cell division regulates the T cell cytokine repertoire, revealing a mechanism underlying immune class regulation. *Proc Natl Acad Sci U S A*. 1998;95(16):9488-93. PubMed PMID: 9689107.
9. Gett AV, Hodgkin PD. A cellular calculus for signal integration by T cells. *Nature immunology*. 2000;1(3):239-44. PubMed PMID: 10973282.
10. Hawkins ED, Turner ML, Dowling MR, van Gend C, Hodgkin PD. A model of immune regulation as a consequence of randomized lymphocyte division and death times. *Proc Natl Acad Sci U S A*. 2007;104(12):5032-7. PubMed PMID: 17360353.
11. Wellard CJ, Markham JF, Hawkins ED, Hodgkin PD, editors. *The Cyton Model for Lymphocyte Proliferation and Differentiation*: Springer; 2011.
12. Macallan DC, Asquith B, Irvine AJ, Wallace DL, Worth A, Ghattas H, et al. Measurement and modeling of human T cell kinetics. *Eur J Immunol*. 2003;33(8):2316-26. doi: 10.1002/eji.200323763. PubMed PMID: 12884307.
13. Yates A, Stark J, Klein N, Antia R, Callard R. Understanding the slow depletion of memory CD4(+) T cells in HIV infection (vol 4, pg e177, 2007). *Plos Med*. 2008;5(1):164-5. doi: ARTN e11 10.1371/journal.pmed.0050011.g002. PubMed PMID: WOS:000254928700023.
14. Green DR, Droin N, Pinkoski M. Activation-induced cell death in T cells. *Immunol Rev*. 2003;193(1):70-81. doi: DOI 10.1034/j.1600-065X.2003.00051.x. PubMed PMID: WOS:000182833700008.
15. den Braber I, Mugwagwa T, Vrisekoop N, Westera L, Mogling R, de Boer AB, et al. Maintenance of peripheral naive T cells is sustained by thymus output in mice but not humans. *Immunity*. 2012;36(2):288-97. doi: 10.1016/j.immuni.2012.02.006. PubMed PMID: 22365666.
16. van Gent R, Kater AP, Otto SA, Jaspers A, Borghans JAM, Vrisekoop N, et al. In vivo dynamics of stable chronic lymphocytic leukemia inversely correlate with somatic hypermutation levels and suggest no major leukemic turnover in bone marrow. *Cancer Res*. 2008;68(24):10137-44.
17. Macallan DC, Fullerton CA, Neese RA, Haddock K, Park SS, Hellerstein MK. Measurement of cell proliferation by labeling of DNA with stable isotope-labeled glucose: studies in vitro, in animals, and in humans. *Proc Natl Acad Sci U S A*. 1998;95(2):708-13. PubMed PMID: 9435257; PubMed Central PMCID: PMC18485.

18. Ho DD, Neumann AU, Perelson AS, Chen W, Leonard JM, Markowitz M. Rapid turnover of plasma virions and CD4 lymphocytes in HIV-1 infection. *Nature*. 1995;373(6510):123-6. PubMed PMID: 7816094.
19. Perelson AS, Neumann AU, Markowitz M, Leonard JM, Ho DD. HIV-1 dynamics in vivo: virion clearance rate, infected cell life-span, and viral generation time. *Science*. 1996;271(5255):1582-6. PubMed PMID: 8599114.
20. Deenick EK, Gett AV, Hodgkin PD. Stochastic model of T cell proliferation: a calculus revealing IL-2 regulation of precursor frequencies, cell cycle time, and survival. *J Immunol*. 2003;170(10):4963-72. PubMed PMID: 12734339.
21. Duffy KR, Wellard CJ, Markham JF, Zhou JH, Holmberg R, Hawkins ED, et al. Activation-induced B cell fates are selected by intracellular stochastic competition. *Science*. 2012;335(6066):338-41. doi: 10.1126/science.1213230. PubMed PMID: 22223740.
22. Dowling MR, Milutinovic D, Hodgkin PD. Modelling cell lifespan and proliferation: is likelihood to die or to divide independent of age? *J R Soc Interface*. 2005;2(5):517-26. PubMed PMID: 16849210.
23. Asquith B, Debacq C, Macallan DC, Willems L, Bangham CR. Lymphocyte kinetics: the interpretation of labelling data. *Trends Immunol*. 2002;23(12):596-601. PubMed PMID: 12464572.
24. Heinzl S, Binh Giang T, Kan A, Marchingo JM, Lye BK, Corcoran LM, et al. A Myc-dependent division timer complements a cell-death timer to regulate T cell and B cell responses. *Nature immunology*. 2016. doi: 10.1038/ni.3598. PubMed PMID: 27820810.
25. Asquith B, de Boer RJ. How lymphocytes add up. *Nat Immunol*. 2016;18(1):12-3. Epub 2016/12/17. doi: 10.1038/ni.3636. PubMed PMID: 27984568.
26. Regoes RR, Barber DL, Ahmed R, Antia R. Estimation of the rate of killing by cytotoxic T lymphocytes in vivo. *Proc Natl Acad Sci U S A*. 2007;104(5):1599-603.
27. Bonhoeffer S, Mohri H, Ho D, Perelson AS. Quantification of cell turnover kinetics using 5-bromo-2'-deoxyuridine. *J Immunol*. 2000;164(10):5049-54. PubMed PMID: 10799860.
28. Barber DL, Wherry EJ, Ahmed R. Cutting edge: rapid in vivo killing by memory CD8 T cells. *J Immunol*. 2003;171(1):27-31. PubMed PMID: 12816979.
29. De Boer RJ, Perelson AS. Quantifying T lymphocyte turnover. *J Theor Biol*. 2013;327:45-87. doi: 10.1016/j.jtbi.2012.12.025. PubMed PMID: 23313150; PubMed Central PMCID: PMC3640348.
30. Asquith B, de Boer RJ. How lymphocytes add up. *Nat Immunol*. 2017;18(1):12-3. doi: 10.1038/ni.3636.
31. Busch R, Neese RA, Awada M, Hayes GM, Hellerstein MK. Measurement of cell proliferation by heavy water labeling. *Nat Protoc*. 2007;2(12):3045-57. doi: 10.1038/nprot.2007.420. PubMed PMID: 18079703.
32. Asquith B, Borghans JA, editors. *Modelling lymphocyte dynamics in vivo*: Springer; 2011.
33. Vriskoop N, den Braber I, de Boer AB, Ruiters AF, Ackermans MT, van der Crabben SN, et al. Sparse production but preferential incorporation of recently produced naive T cells in the human peripheral pool. *Proc Natl Acad Sci U S A*. 2008;105(16):6115-20. PubMed PMID: 18420820.
34. De Boer RJ, Mohri H, Ho DD, Perelson AS. Turnover rates of B cells, T cells, and NK cells in simian immunodeficiency virus-infected and uninfected rhesus macaques. *J Immunol*. 2003;170(5):2479-87. PubMed PMID: 12594273.
35. Costa Del Amo P, Lahoz-Beneytez J, Boelen L, Ahmed R, Miners KL, Zhang Y, et al. Human TSCM cell dynamics in vivo are compatible with long-lived immunological memory and stemness. *PLOS Biol*. 2018;16(6):e2005523. doi: 10.1371/journal.pbio.2005523. PubMed PMID: 29933397; PubMed Central PMCID: PMC6033534.
36. Patel AA, Zhang Y, Fullerton JN, Boelen L, Rongvaux A, Maini AA, et al. The fate and lifespan of human monocyte subsets in steady state and systemic inflammation. *J Exp Med*. 2017;214(7):1913-23. doi: 10.1084/jem.20170355. PubMed PMID: 28606987; PubMed Central PMCID: PMC605502436.
37. Lahoz-Beneytez J, Schaller S, Macallan D, Eissing T, Niederaalt C, Asquith B. Physiologically Based Simulations of Deuterated Glucose for Quantifying Cell Turnover in Humans. *Front Immunol*.

- 2017;8:474. doi: 10.3389/fimmu.2017.00474. PubMed PMID: 28487698; PubMed Central PMCID: PMC5403812.
38. Lahoz-Beneytez J, Elemans M, Zhang Y, Ahmed R, Salam A, Block M, et al. Human neutrophil kinetics: modeling of stable isotope labeling data supports short blood neutrophil half-lives. *Blood*. 2016;127(26):3431-8. doi: 10.1182/blood-2016-03-700336. PubMed PMID: 27136946; PubMed Central PMCID: PMC4929930.
39. Younes SA, Punkosdy G, Caucheteux S, Chen T, Grossman Z, Paul WE. Memory phenotype CD4 T cells undergoing rapid, nonburst-like, cytokine-driven proliferation can be distinguished from antigen-experienced memory cells. *PLOS Biol*. 2011;9(10):e1001171. Epub 2011/10/25. doi: 10.1371/journal.pbio.1001171. PubMed PMID: 22022231; PubMed Central PMCID: PMC3191130.
40. Gossel G, Hogan T, Cownden D, Seddon B, Yates AJ. Memory CD4 T cell subsets are kinetically heterogeneous and replenished from naive T cells at high levels. *Elife*. 2017;6. Epub 2017/03/11. doi: 10.7554/eLife.23013. PubMed PMID: 28282024; PubMed Central PMCID: PMC5426903.
41. Burnham KP, Anderson DR. *Model selection and multimodel inference*. New York, NY: Springer-Verlag; 2002.
42. Saraste A. Morphologic criteria and detection of apoptosis. *Herz*. 1999;24(3):189-95. PubMed PMID: WOS:000080613700002.
43. Zhang GH, Gurtu V, Kain SR, Yan GC. Early detection of apoptosis using a fluorescent conjugate of annexin V. *Biotechniques*. 1997;23(3):525-&. PubMed PMID: WOS:A1997XW10200033.
44. Hasper HJ, Weghorst RM, Richel DJ, Meerwaldt JH, Olthuis FMFG, Schenkeveld CEI. A new four-color flow cytometric assay to detect apoptosis in lymphocyte subsets of cultured peripheral blood cells. *Cytometry*. 2000;40(2):167-71. doi: 10.1002/(sici)1097-0320(20000601)40:2<167::aid-cyto11>3.0.co;2-1.
45. Segawa K, Suzuki J, Nagata S. Constitutive exposure of phosphatidylserine on viable cells. *Proceedings of the National Academy of Sciences of the United States of America*. 2011;108(48):19246-51. doi: 10.1073/pnas.1114799108. PubMed PMID: 22084121; PubMed Central PMCID: PMC3228483.
46. Elliott JI, Surprenant A, Marelli-Berg FM, Cooper JC, Cassady-Cain RL, Wooding C, et al. Membrane phosphatidylserine distribution as a non-apoptotic signalling mechanism in lymphocytes. *Nat Cell Biol*. 2005;7(8):808-16. doi: 10.1038/ncb1279. PubMed PMID: 16025105.
47. Cotter TG, al-Rubeai M. Cell death (apoptosis) in cell culture systems. *Trends Biotechnol*. 1995;13(4):150-5. Epub 1995/04/01. doi: 10.1016/s0167-7799(00)88926-x. PubMed PMID: 7766111.
48. Heinzl S, Binh Giang T, Kan A, Marchingo JM, Lye BK, Corcoran LM, et al. A Myc-dependent division timer complements a cell-death timer to regulate T cell and B cell responses. *Nat Immunol*. 2017;18(1):96-103. doi: 10.1038/ni.3598. PubMed PMID: 27820810.
49. Barsov EV. Telomerase and primary T cells: biology and immortalization for adoptive immunotherapy. *Immunotherapy*. 2011;3(3):407-21. Epub 2011/03/15. doi: 10.2217/imt.10.107. PubMed PMID: 21395382; PubMed Central PMCID: PMC3120014.
50. Vibert J, Thomas-Vaslin V. Modelling T cell proliferation: Dynamics heterogeneity depending on cell differentiation, age, and genetic background. *PLOS Comput Biol*. 2017;13(3):e1005417. Epub 2017/03/14. doi: 10.1371/journal.pcbi.1005417. PubMed PMID: 28288157; PubMed Central PMCID: PMC5367836.
51. Boelen L, Debebe B, Silveira M, Salam A, Makinde J, Roberts CH, et al. Inhibitory killer cell immunoglobulin-like receptors strengthen CD8(+) T cell-mediated control of HIV-1, HCV, and HTLV-1. *Sci Immunol*. 2018;3(29). doi: 10.1126/sciimmunol.aao2892. PubMed PMID: 30413420.
52. Marchingo JM, Kan A, Sutherland RM, Duffy KR, Wellard CJ, Belz GT, et al. T cell signaling. Antigen affinity, costimulation, and cytokine inputs sum linearly to amplify T cell expansion. *Science*. 2014;346(6213):1123-7. doi: 10.1126/science.1260044. PubMed PMID: 25430770.
53. Dowling MR, Hodgkin PD. Why does the thymus involute? A selection-based hypothesis. *Trends Immunol*. 2009;30(7):295-300. doi: 10.1016/j.it.2009.04.006. PubMed PMID: 19540805.

54. Dowling MR, Hodgkin PD. Modelling naive T-cell homeostasis: consequences of heritable cellular lifespan during ageing. *Immunol Cell Biol.* 2009;87(6):445-56. doi: 10.1038/icb.2009.11. PubMed PMID: 19290017.
55. Flossdorf M, Rossler J, Buchholz VR, Busch DH, Hofer T. CD8+ T cell diversification by asymmetric cell division. *Nat Immunol.* 2015;16(9):891-3. doi: 10.1038/ni.3235  
<http://www.nature.com/ni/journal/v16/n9/abs/ni.3235.html#supplementary-information>.
56. Baker CTH, Bocharov GA, Ford JM, Lumb PM, Norton SJ, Paul CAH, et al. Computational approaches to parameter estimation and model selection in immunology. *Journal of Computational and Applied Mathematics.* 2005;184(1):50-76. doi: <http://dx.doi.org/10.1016/j.cam.2005.02.003>.
57. Cantrell DA, Smith KA. The interleukin-2 T-cell system: a new cell growth model. *Science.* 1984;224(4655):1312-6. PubMed PMID: 6427923.
58. Soetaert K. R Package FME : Inverse Modelling, Sensitivity, Monte Carlo – Applied to a Dynamic Simulation Model. URL <https://cran.r-project.org/web/packages/FME/>.
59. Burnham KP, Anderson DR. Model selection and multi-model inference. New York, NY: Springer; 2002.

## Figures

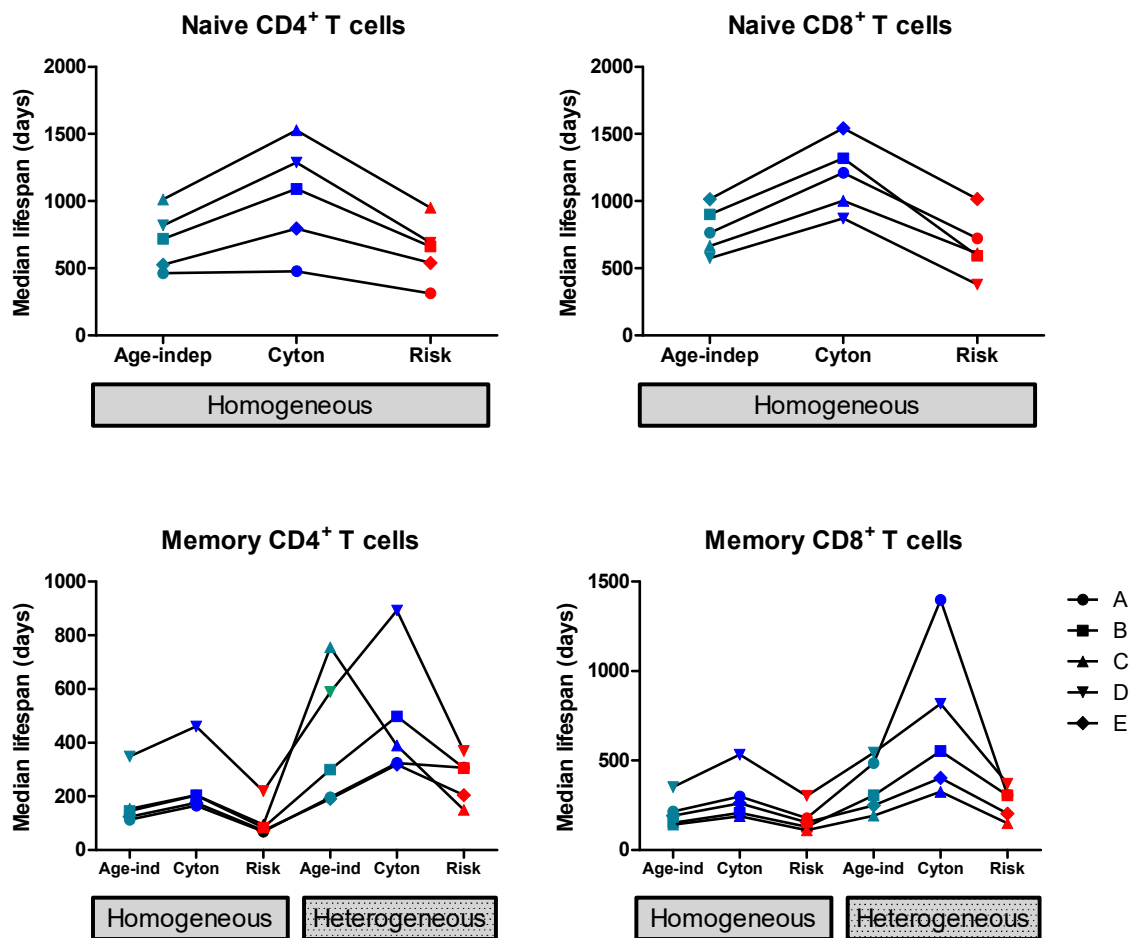
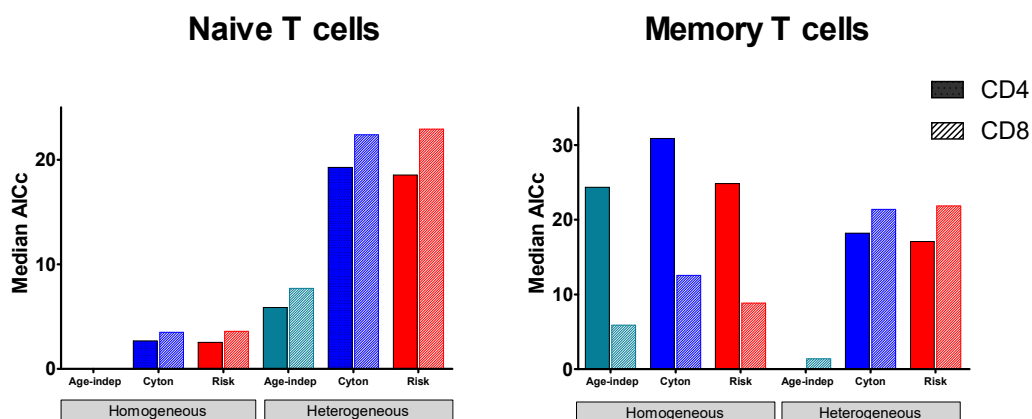


**Figure 1. Impact of model assumptions on lifespan estimates.**

Median lifespan estimates obtained by fitting models with different assumptions about cell fate to heavy water labelling data [33]. Top row: naive T cells, bottom row: memory T cells. Each line and symbol corresponds to a different subject (A-E). Here the cyton and risk models are described using the gamma distribution, similar results are obtained using the lognormal distribution. We use the colour scheme age-independent: aqua, cyton: cobalt, risk: red. The lifespan of a cell is defined as the time to first event (division or death).

## A. Age-dependent models described by gamma distribution



## B. Age-dependent models described by lognormal distribution

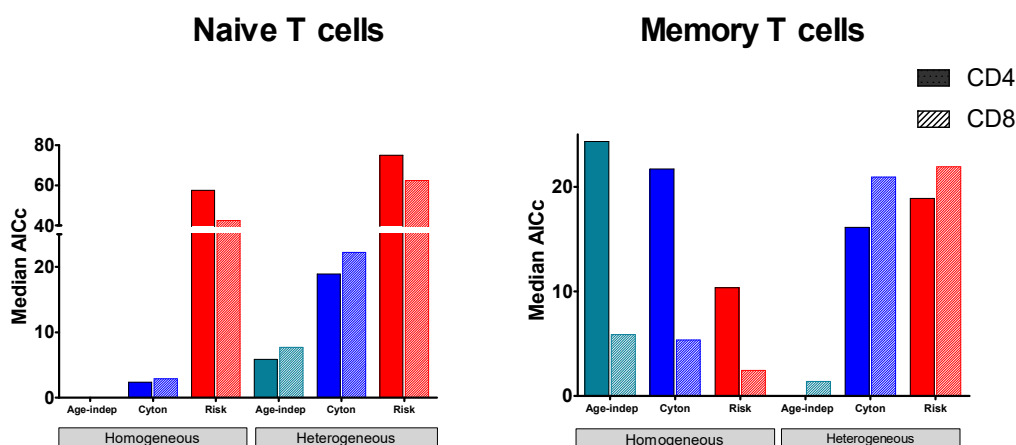
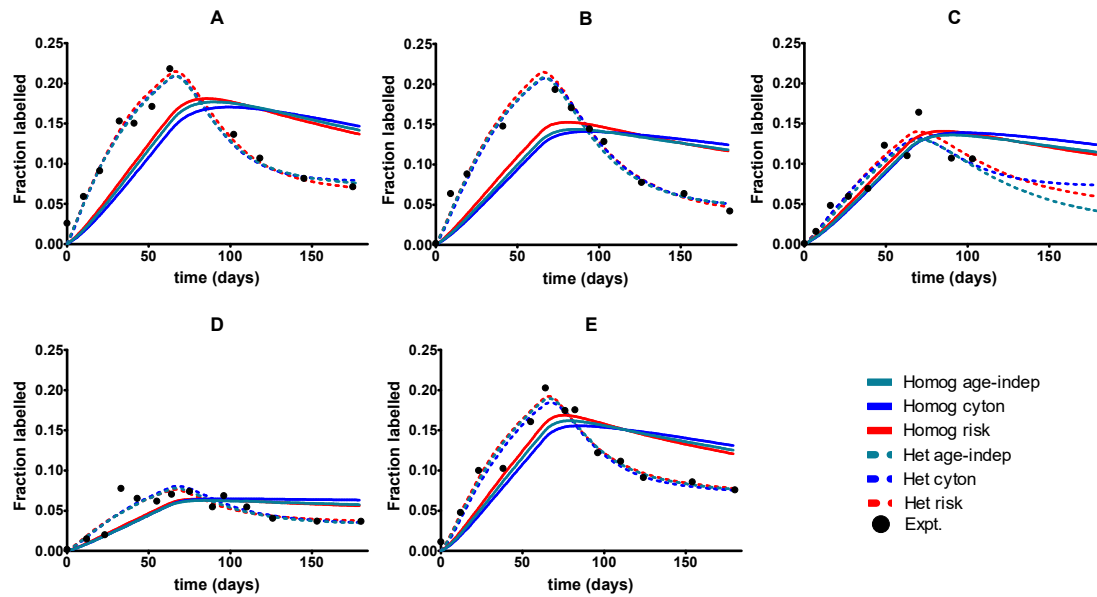


**Figure 2. Median normalised AICc for the fit of each of the models to data from naïve and memory CD4<sup>+</sup> and CD8<sup>+</sup> T cells.** The model with the lowest AICc is the best performing model. The age-independent model performs best both for naïve CD4<sup>+</sup> and CD8<sup>+</sup> T cells (homogeneous version) and for memory CD4<sup>+</sup> and CD8<sup>+</sup> T cells (heterogeneous version). The data fitted is from the heavy water study. **A** shows median normalised AICc for the gamma versions of the age-dependent models; **B** shows median normalised AICc for the lognormal versions of the age-dependent models. The individual AICc values are in **Supplementary Table S1** and **S2**. We use the colour scheme age-indep: aqua, cyton: cobalt, risk: red; solid colour in bars denotes CD4<sup>+</sup> cells, hatched colour denotes CD8<sup>+</sup> cells. Note the y axis scales are different in each panel (and broken in one panel). Absolute value of the AICc does not carry any meaning so we plot the normalised AICc which is the difference between the AICc of the model being investigated and the winning model (the normalised AICc is therefore zero for the winning model).

## A. Memory CD4<sup>+</sup> T cells



## B. Memory CD8<sup>+</sup> T cells

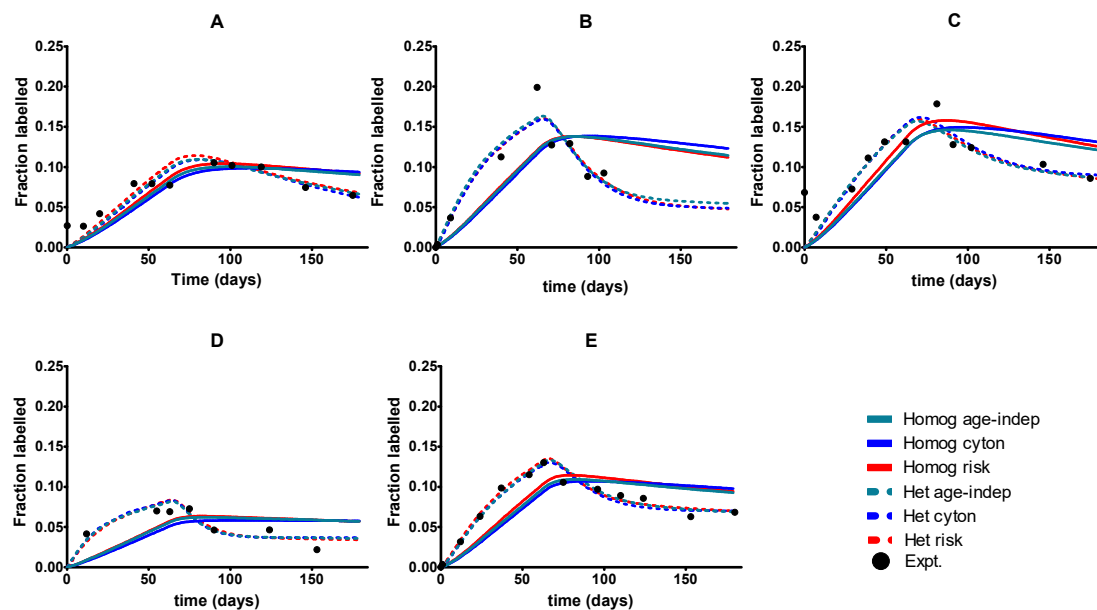


**Figure 3. Best fit of the 6 models to Memory CD8<sup>+</sup> and CD4<sup>+</sup> T cell data.**

A different subject (A-E) is shown in each panel. Here the cyton and risk models are described using the gamma distribution; similar results are obtained using the lognormal distribution. We use the colour scheme age-independent: aqua, cyton: cobalt, risk: red; solid lines denote best fit of homogeneous models, dashed lines best fit of heterogeneous models; black circles denote experimental data. Data taken from [33].

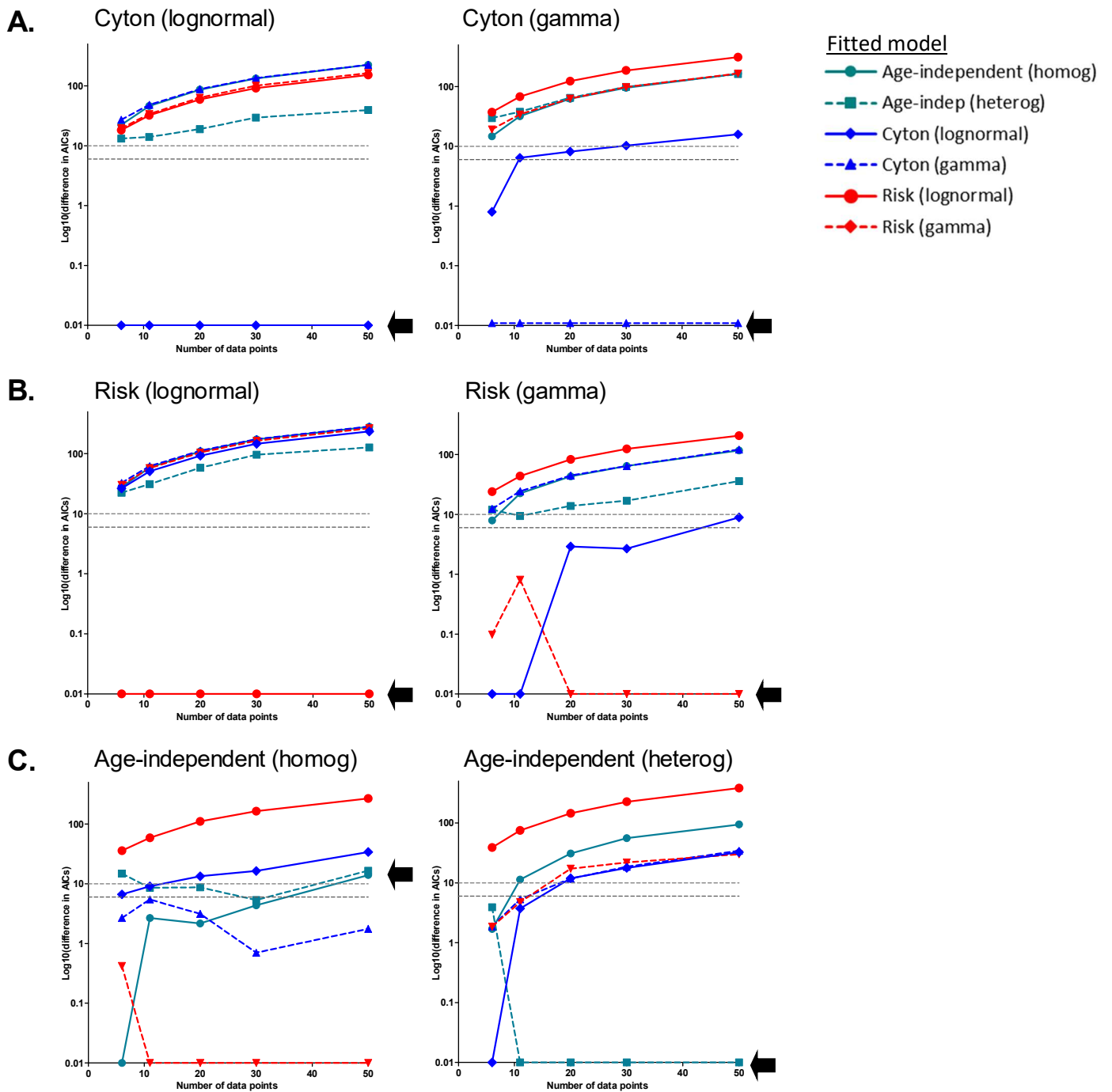


**Figure 4. Approach Validation.**

*In silico* data (with noise) was generated using the paradigm named above each panel. Datasets of different sizes ( $n=6$ ,  $n=11$ ,  $n=20$ ,  $n=30$ ,  $n=50$ ) were constructed;  $n=11$  corresponds to the typical size of experimental data set analysed in the previous section. We then used our approach to identify the generating model. Briefly, each of the models was fitted to the data and the normalised AICc is plotted. The normalised AICc for the winning model (which is zero by definition) is plotted as 0.01 since  $\log_{10}(0)$

is not defined. In each panel a different model was used to generate the data (generating model is named above each panel), each line represents the normalised AICc from fitting a different model to the generated data, the x axis is the size of the data set; the AICc of the generating model is indicated by a black arrow. The model with the lowest normalised AICc is the model identified as the generating model by our approach. **A.** Generating model is the cyton model (either lognormal or gamma). The generating model was always correctly identified (lowest AICc) (with the exception of one model for the smallest dataset  $n=6$ ) no other model came within 6 AICc of the generating model (. **B.** Generating model is the risk model. For the lognormal version the generating model was always correctly identified; for the gamma version the generating model was correctly identified the majority of the time and when it was not the winning model it was always within 1 AICc of the winning model (i.e. it was indistinguishable from the winning model). **C.** Generating model is the age-independent model. For the age-independent heterogeneous model the winning model was the generating model for  $n \geq 11$ , though for  $n=11$  (but not higher) other models were competitive. For the age-independent homogeneous model the winning model for most values of  $n$  was, unexpectedly, gamma risk. The grey dashed horizontal lines correspond to a difference in AICc of 6 and 10, these are the rule of thumb cutoffs typically used with the AICc. A difference of 6 is considered sufficient to support the winning model, a difference of 10 allows the favouring of the winning model with confidence.

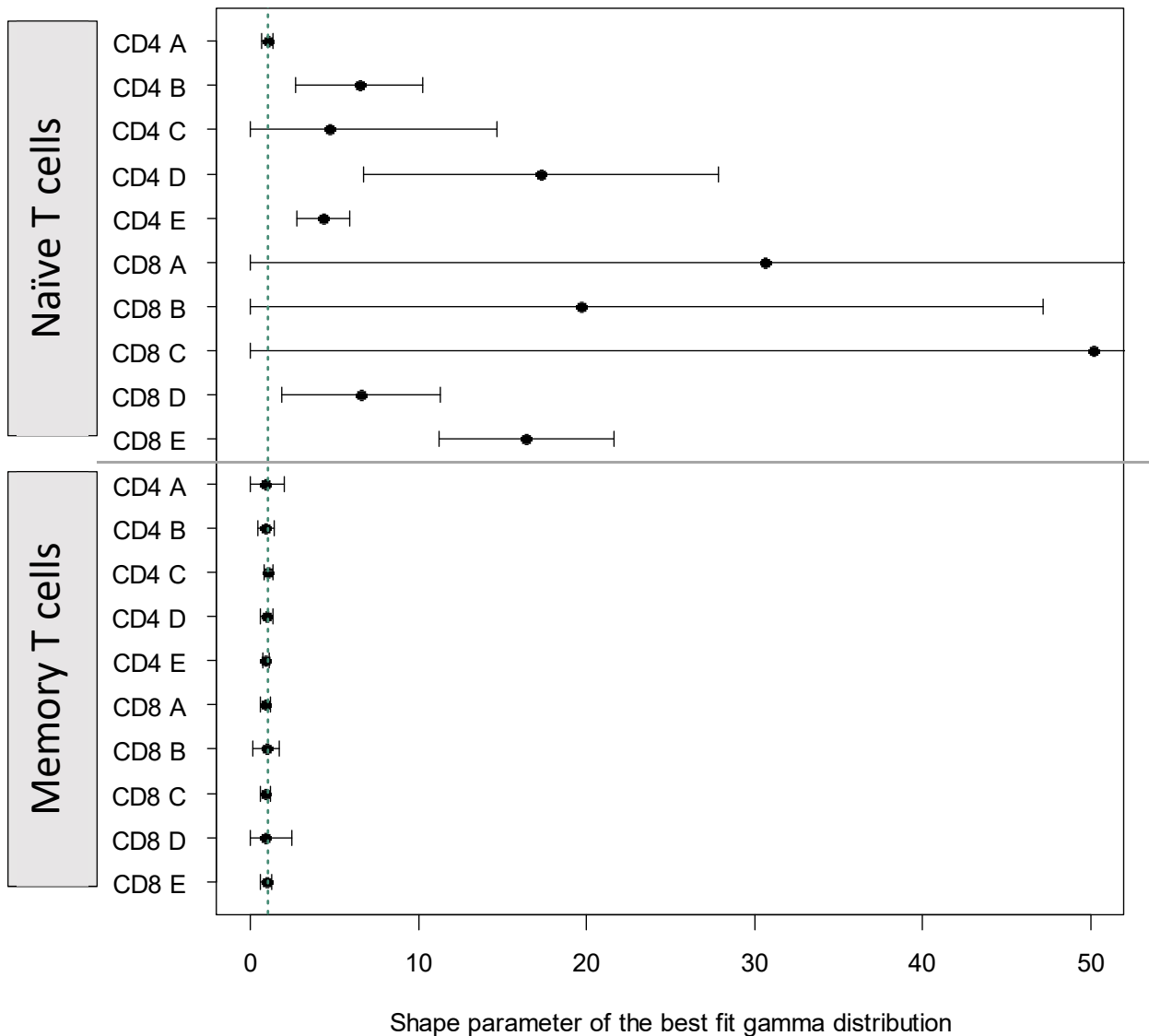
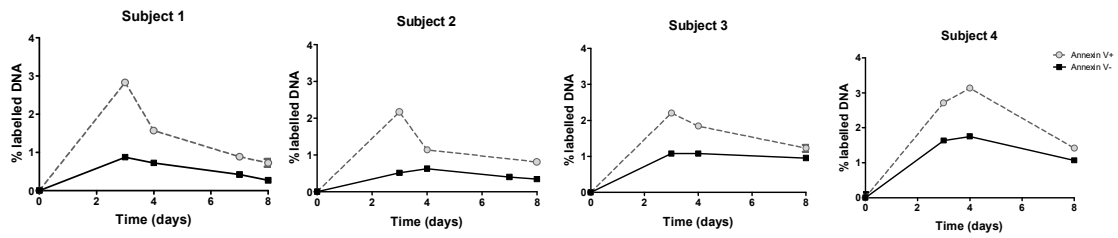


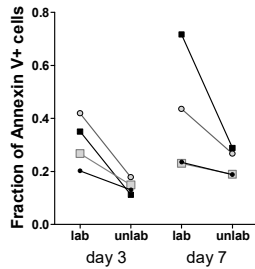
**Figure 5. Alternative approach: shape parameter of the best fit gamma distribution.**

We fitted a model in which time to death/differentiation and time to division were drawn from gamma distributions with unconstrained shape and scale parameters. The model thus has the freedom to take up the risk paradigm ( $\text{shape} < 1$ ), the age-independent paradigm ( $\text{shape} = 1$ ) or the cyton paradigm ( $\text{shape} > 1$ ). The shape parameter of the best fit distributions to each of the cell populations is plotted above. Vertical green dashed line corresponds to  $\text{shape} = 1$ . The first 10 estimates (above the horizontal line) are for naïve T cells, the next 10 estimates (below the horizontal line) are for memory T cells.

## A. Raw experimental data



## B. Observed signature in experimental data



## C. Predicted signature

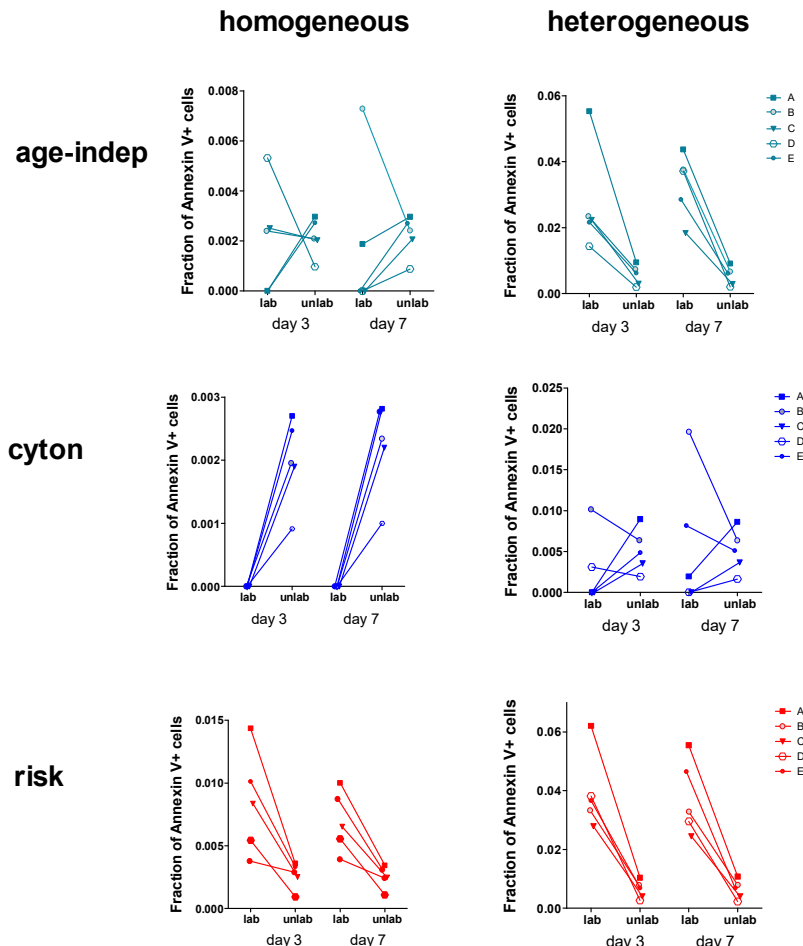


**Figure 6. Observed and predicted signatures in Annexin V data set.**

**A.** Four subjects were labelled with deuterated glucose for 24h. The fraction of labelled DNA in Annexin V+ and Annexin V- CD4<sup>+</sup>CD45RO<sup>+</sup> T cells was quantified (one subject per graph). **B.** This was converted into a signature of the fraction of Annexin V+ cells amongst labelled and unlabelled cells. **C.** We tested the ability of each of the 6 models to predict this signature; the heterogeneous age-independent and both homogeneous and heterogeneous risk models correctly predicted the signature; the homogeneous age-independent, homogeneous cyton and heterogeneous cyton models did not.

## Boxes

Age of a cell	Time since cell was created by division (“born”) i.e. mitosis results in two daughter cells both of age 0 days.
Lifespan of a cell	Time from creation of a cell by division to its loss by division, death or differentiation.
Age-independent fate	The probability of a cell’s death, differentiation or division is independent of its age
Birth of a cell	Creation of a cell by division of the mother cell

### Box 1. Definition of terms

## Tables

Model	Paradigm	Number of subpopulations	Distribution of time to die and divide	Number of free parameters
1. Age-independent, homogeneous	Age-independent	1	exponential (gamma with shape=1)	1
2. Age-independent, heterogeneous		2	exponential (gamma with shape=1)	3
3. Cyton, homogeneous	Cyton	1	gamma or lognormal	2
4. Cyton, heterogeneous		2	gamma or lognormal	5
5. Risk, homogeneous	Risk	1	gamma or lognormal	2
6. Risk, heterogeneous		2	gamma or lognormal	5

**Table 1. Summary of the different models considered**

The number of kinetically distinct subpopulations, type of distribution for times to die/differentiate and to divide, and number of free parameters for each of the 6 models. We considered 3 paradigms (age-independent, cyton, risk); 6 models (i.e. homogeneous and heterogeneous versions of each paradigm) with 10 formulations in total (as each of the age-dependent models can be described either by the gamma or the lognormal distribution).

## Supplementary Information

### Derivation of the pdf of remaining lifetime at equilibrium

#### Motivation

In an age-dependent model the remaining lifetime of the population will evolve over time as the population ages. We assume that as we are labelling adults the system has reached steady state. We therefore wish to determine the steady state distribution of remaining lifetimes in order to initialise the ABM model.

#### Definitions

**Source distribution** New cells are born with age 0 and assigned a time to die and a time to divide which are random variables taken from a predetermined distribution, following Hodgkin et al. we refer to this predetermined distribution as the source distribution. The source distribution is assumed to take the same form and parameters for both death and division to achieve homeostasis. We denote the pdf of the source distribution  $f(x)$  and the associated probability  $P(X)$ . That is the probability that a cell divides between age  $a$  and age  $b$  is denoted

$$P(a \leq x \leq b) = \int_a^b f(x)dx.$$

**Censored source distribution** The censored source distribution describes the time to the first event (death or division whichever occurs first), we denote the pdf  $f_c(x)$  and the associated probability  $P_C(X)$ . That is the probability that the first event (death or division) occurs between age  $a$  and age  $b$  is denoted

$$P_C(a \leq x \leq b) = \int_a^b f_C(x)dx.$$

**Remaining lifetime distribution** The remaining lifetime distribution describes the distribution of remaining lifetimes i.e. distribution of [time to the first event - age of the cell]. We denote the pdf  $f_R(x, t)$  and the associated probability  $P_R(X, t)$ . That is the probability that at time  $t$  the remaining lifetime is between  $a$  and  $b$  is denoted

$$P_R(a \leq x \leq b, t) = \int_a^b f_R(x, t)dx.$$

Note that, with the exception of the case when the source is exponentially distributed, the remaining lifespan distribution will depend on time. The remaining lifespan distribution at time  $t=0$  is equal to the censored source distribution;  $P_R(X = x, t = 0) = P_C(X = x)$ .

#### Deriving the pdf of the censored distribution

Let  $X$  be the RV time to die,  $Y$  the RV time to divide and  $Z$  the RV time to first event; then

$$\begin{aligned} P(Z = z) &= P(X = z)P(Y > z) + P(X > z)P(Y = z) \\ &= 2P(X = z)P(Y > z) \\ &= 2P(X = z)[1 - P(Y \leq z)] \end{aligned}$$

That is the pdf of the censored distribution is just twice the  $pdf \times (1 - cdf)$  of the source distribution.

## Deriving the pdf of the remaining lifetime at equilibrium

Consider the evolution of the probability that a cell has remaining lifespan  $\lambda$  from probability at time  $t$ ,  $p_R(\lambda, t)$  to the probability at time  $t + \Delta t$ ,  $p_R(\lambda, t + \Delta t)$

$$p_R(\lambda, t + \Delta t) = p_R(\lambda + \Delta t, t) + \int_{z=0}^{\Delta t} p_R(z, t) dz p_R(\lambda, 0) \quad (1)$$

Consider (1) at time such that have reached steady state. Denote the distribution of lifetimes at equilibrium  $p_R^*(\lambda, t)$ , obviously independent of  $t$ , left in for consistency. Now  $p_R^*(\lambda, t + \Delta t) = p_R^*(\lambda, t)$  (the definition of steady state) and  $\int_{z=0}^{\Delta t} p_R^*(z, t) dz \approx p_R^*(0, t) \Delta t$  in (1) at s.s. gives

$$\begin{aligned} p_R^*(\lambda, t) &= p_R^*(\lambda + \Delta t, t) + p_R^*(0, t) \Delta t p_R(\lambda, 0) \\ \frac{p_R^*(\lambda, t) - p_R^*(\lambda + \Delta t, t)}{\Delta t} &= p_R^*(0, t) p_R(\lambda, 0) \end{aligned}$$

take  $\lim \Delta t \rightarrow 0$

$$-\frac{dp_R^*(\lambda, t)}{d\lambda} = p_R^*(0, t) p_R(\lambda, 0)$$

$$p_R^*(\lambda, t) = - \int_{z=0}^{\lambda} p_R^*(0, t) p_R(z, 0) dz + C$$

setting  $\lambda = 0$  gives  $C = p_R^*(0, t)$  so

$$p_R^*(\lambda, t) = p_R^*(0, t) \left[ 1 - \int_{z=0}^{\lambda} p_R(z, 0) dz \right] \quad (2)$$

$p_R^*(\lambda, t)$  is a pdf so integrates to 1. That is

$$p_R^*(0, t) = \frac{1}{\int_{\lambda=0}^{\infty} 1 - \int_{z=0}^{\lambda} p_R(z, 0) dz d\lambda}$$

consider the denominator

$$\int_{\lambda=0}^{\infty} 1 - \int_{z=0}^{\lambda} p_R(z, 0) dz d\lambda = \mu_C$$

where  $\mu_C$  is the expectation of the remaining lifetime distribution at time zero (ie the censored source distribution). Since  $\int_{\lambda=0}^{\infty} 1 - F(\lambda) d\lambda = E[\lambda]$  where  $F$  is the cdf and  $E$  the expectation of any continuous pdf which is zero when  $z \leq 0$ .

So  $p_R^*(0, t) = 1/\mu_C$  and from (2)

$$p_R^*(\lambda, t) = \frac{1}{\mu_C} \left[ 1 - \int_{z=0}^{\lambda} p_R(z, 0) dz \right] \quad (3)$$

Unexpectedly, can see that whatever the censored source distribution  $p_R(z, 0)$  the pdf of the remaining lifetime at steady state is monotonic decreasing in  $\lambda$ .

### **Further details of the agent-based model**

The proposed agent-based model (ABM) represents death and division events by sampling times to die or to divide drawn from a gamma or lognormal distribution. This sampling scheme offers a flexible way to simulate stochastic cell population dynamics and is related to several existing quantitative models for T cell population dynamics. Here, we discuss these relations.

#### ***Equivalence of the ABM to deterministic models & the Gillespie algorithm***

In general, stochastic birth-death Poisson processes for a sufficiently large population size would be expected to exhibit equivalent population dynamics to that generated by a deterministic equation [S1]. We have confirmed that the homogeneous age-independent model, as a special case of the ABM, is technically equivalent to the conventional Gillespie algorithm. Additionally, we demonstrated that the homogeneous age-independent version of the ABM can fit to the heavy water labelling data of several cell types essentially the same as the deterministic ordinary differential equation formulation of an age-independent process (**Figure 3** and data not shown).

#### ***Relationship of the ABM to the cyton model***

In [S2], it is shown that several existing mathematical models that describe T and B cell population dynamics measured by CFSE labeling can be reformulated as a system of integral equations. The cyton model is included as a special case of their proposed model. In [S3] it is demonstrated that the sampling scheme employed in the ABM can produce a stochastic representation of the population dynamics exhibited by the integral equations of [S2]. In other words, our ABM can formally reproduce population dynamics of the cyton model as stochastic sample paths when distributions for times to die and to divide are chosen to be those assumed in the cyton model.

#### ***A mathematical condition that ensures maintenance of steady state***

Experimental data were taken from adults in which the cell population has reached a steady state. We therefore constrained the distributions of times to die and to divide in the ABM to maintain a constant population size. In [S3], a generation progression ratio was introduced to quantitatively describe the ratio of population sizes between two successive generations. The population size remains constant if generation progression ratios between any of two successive generations are equal to one. This condition is satisfied if times to die and to divide are taken from identical distributions (i.e. same distribution, same parameters). We also relaxed this assumption by allowing times to divide and die to be drawn from the same family of distributions but with different parameters governing the two distributions. In this case steady state was maintained by constraining the expected values of both distributions to be the same. We show numerically that this is sufficient to maintain steady state.

#### ***Determination of feasible initial population size in agent-based simulations***

The ABM produces stochastic sample paths due to the finite number of individuals in the population. This stochasticity may affect the quality of fitting. To determine feasible population sizes that produce stable fits the homogeneous age-independent model with different initial population sizes was fitted to *in vivo* deuterium water labeling data of granulocytes and T cells. Stable estimates were obtained when initial population sizes are greater than 1000 (results not shown). We chose a population size of 10,000. To further minimize the effect of the stochasticity on those estimates, the median cost of five labelling curves generated with five different seeds was considered in each iteration of the fitting process. It should be noticed that we do not use an ABM to simulate the stochasticity of the system

but because it provides a flexible way to incorporate different cell fate models; a deterministic approach such as partial differential equations would be another option.

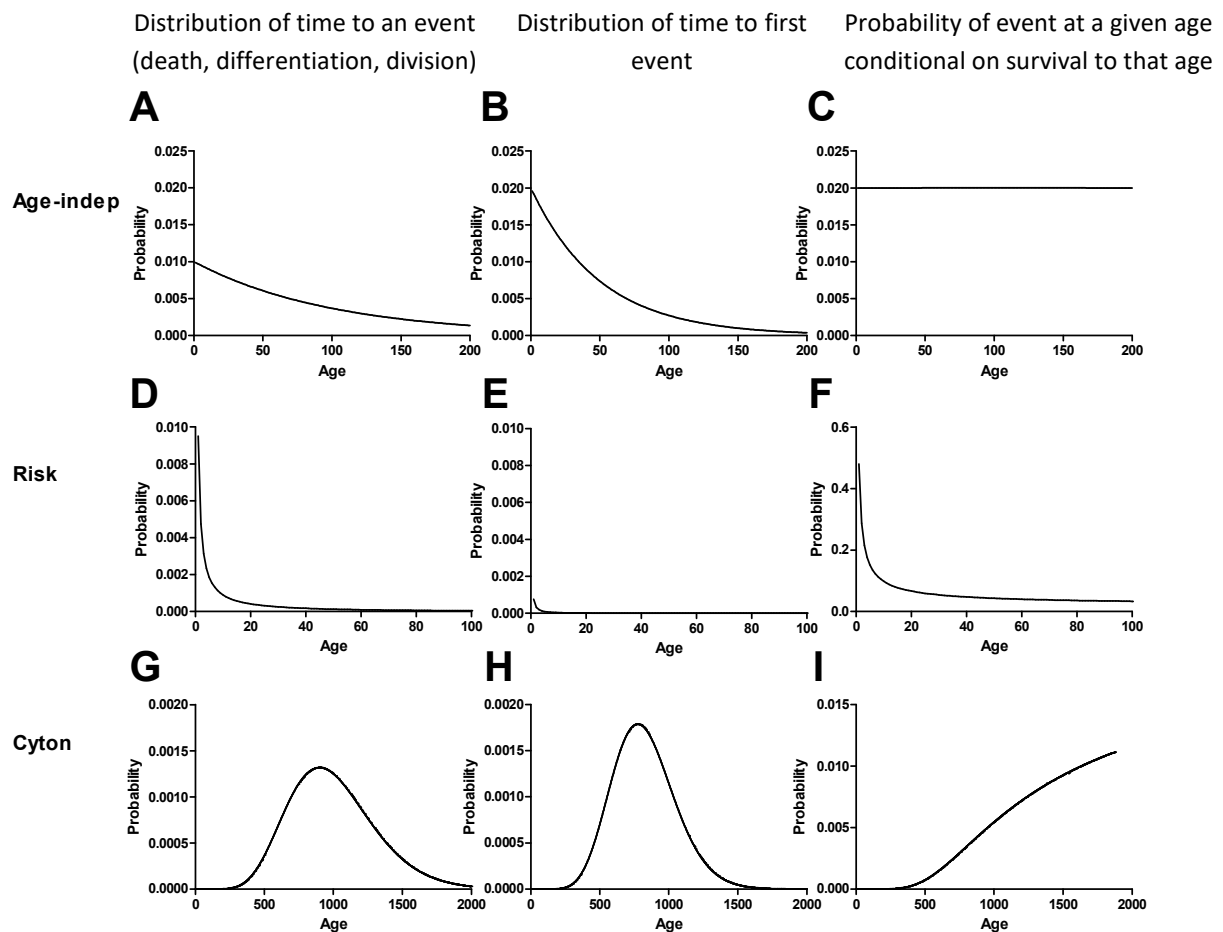
### **References for Supplementary Information**

[S1] D.T. Gillespie, Stochastic Simulation of Chemical Kinetics, *Annual Review of Physical Chemistry* 58 (2007) 35--55.

[S2] A. Zilman, V. V. Ganusov and A. S. Perelson, Stochastic models of lymphocyte proliferation and death, *PLoS One*, 5 (2010), e12775.

[S3] S. Nakaoka and H. Inaba, Demographic modeling of transient amplifying cell population growth, *Mathematical Biosciences and Engineering*, 11(2) (2014) 363-384.

## Supplementary Figures



### Supplementary Figure S1. Examples of lifespan distributions and conditional probability for age-independent and age-dependent paradigms.

For each of the three paradigms: age-independent, risk and cyton (row 1, 2 and 3 respectively) the distribution of time to an event (death, differentiation and division, first column), distribution of time to any event (second column) and instantaneous probability of an event at a given age conditioned on survival to that age (third column) are plotted. In the Supplementary Information the distribution of time to an event is referred to as the source distribution and the distribution of time to any event is referred to as the censored source distribution. In all cases the underlying (source) distribution is the gamma distribution.

**A.** Probability distribution of the time to an event for an age-independent distribution (gamma with shape=1 and rate=0.01, equivalent to exponential with rate=0.01). **B.** Probability distribution of the time to the first event (death, differentiation or division) for an age-independent distribution (gamma with shape=1 and rate=0.01). **C.** Probability of an event occurring immediately after age on x axis given survival to that age for an age-independent distribution (gamma with shape=1 and rate=0.01). **D, E, F** as for **A, B, C** but for an age-dependent distribution consistent with the risk paradigm (gamma with shape=0.01 and rate=0.01). **G, H, I** as for **A, B, C** but for an age-dependent distribution consistent with the cyton paradigm (gamma with shape=10 and rate=0.01). Note the different scales of the x axis and y axis in the different panels.

It can be seen that for the age-independent model the probability of an event at age  $x$  (given survival to age  $x$ ) is independent of age (**C**), for the risk model the probability is highest at birth and then

decreases with age (**F**) and for the cyton model the probability is initially zero and increases with age (**I**).

The functions plotted are as follows

Probability of an event at age  $x$ : 
$$P(x) = \frac{1}{\theta^\alpha \Gamma(\alpha)} x^{\alpha-1} e^{-x/\theta}$$

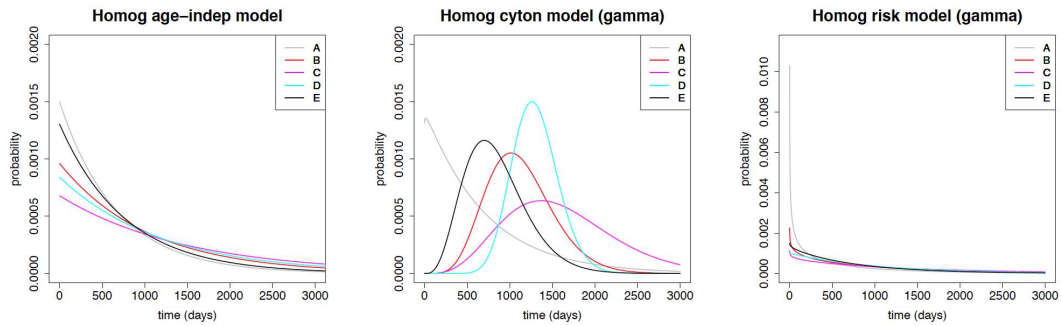
Probability of any event (death/differentiation or division) at age  $x$ :

$$P(x) = 2 \frac{1}{\theta^\alpha \Gamma(\alpha)} x^{\alpha-1} e^{-x/\theta} \int_{y=x}^{\infty} \frac{1}{\theta^\alpha \Gamma(\alpha)} y^{\alpha-1} e^{-y/\theta} dy$$

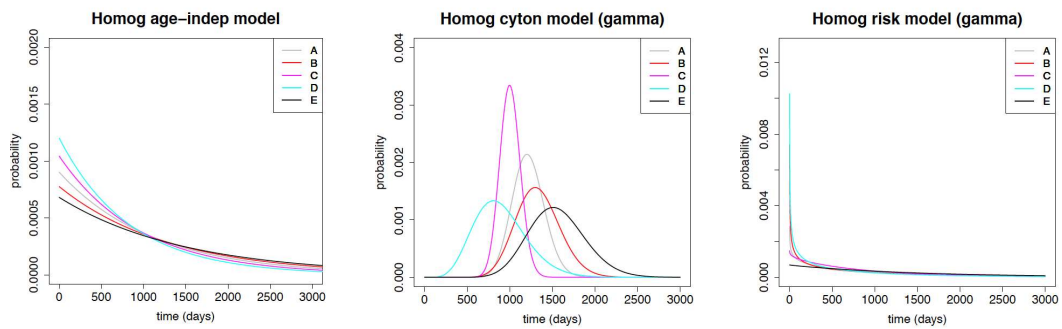
Probability of any event (death/ differentiation or division) at age  $x$  given survival to age  $x$ :

$$P(x) = 2 \frac{1}{\theta^\alpha \Gamma(\alpha)} x^{\alpha-1} e^{-x/\theta} \int_{y=x}^{\infty} \frac{1}{\theta^\alpha \Gamma(\alpha)} y^{\alpha-1} e^{-y/\theta} dy \div \left[ \int_{z=x}^{\infty} \left( 2 \frac{1}{\theta^\alpha \Gamma(\alpha)} z^{\alpha-1} e^{-z/\theta} \int_{y=x}^{\infty} \frac{1}{\theta^\alpha \Gamma(\alpha)} y^{\alpha-1} e^{-y/\theta} dy \right) dz \right]$$

## Naïve CD4<sup>+</sup> T cells



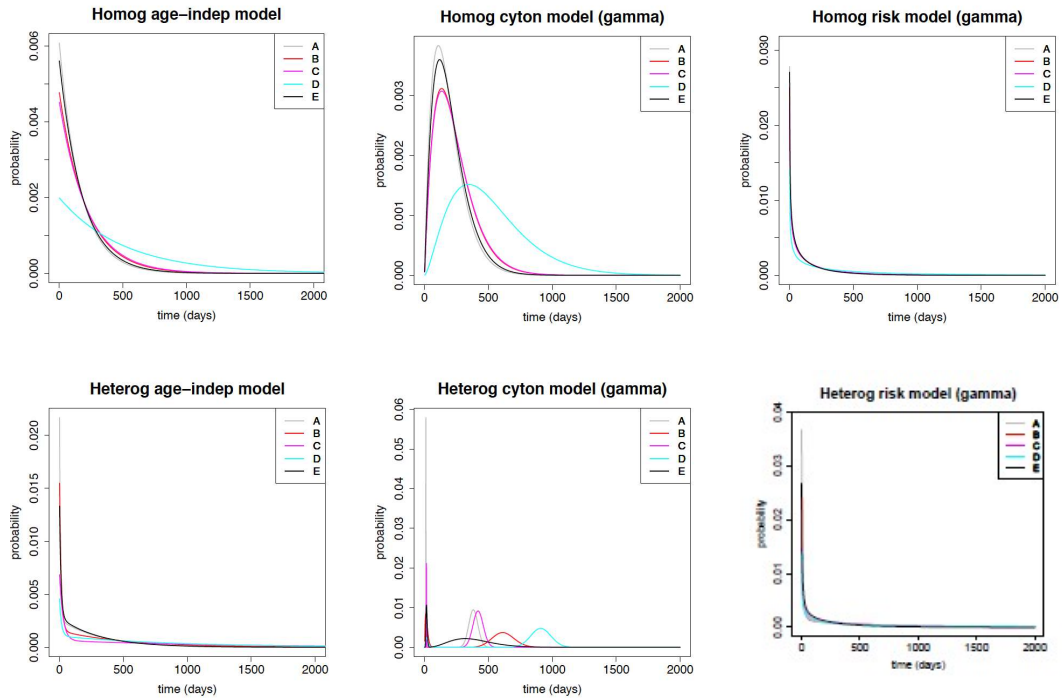
## Naïve CD8<sup>+</sup> T cells



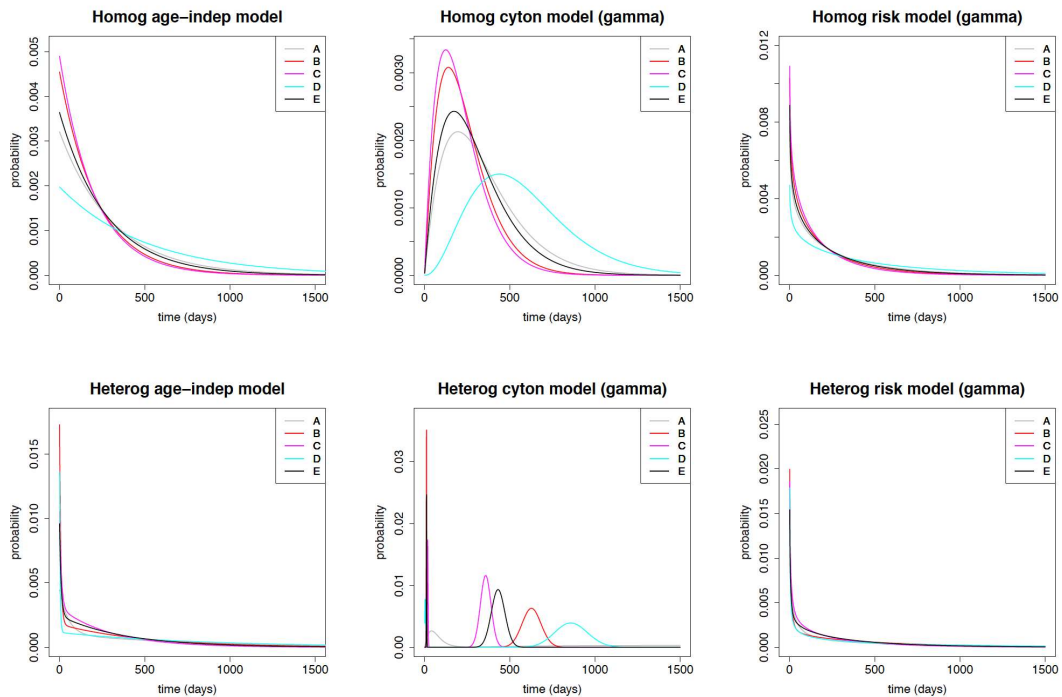
### Supplementary Figure S2. Best fit distributions for naïve T cells.

The experimental data from 5 individuals (A-E) from the heavy water study were fitted with the homogeneous version of the three paradigms (age-independent, cyton and risk). The best fit censored lifespan distributions (i.e. the distribution of the time from cell birth by division of the mother cell to either death or division whichever occurs first) are plotted. Top row shows the best fits for naïve CD4<sup>+</sup> T cells and bottom row the best fits for naïve CD8<sup>+</sup> T cells. Each coloured curve corresponds to a different individual.

## Memory CD4<sup>+</sup> T cells



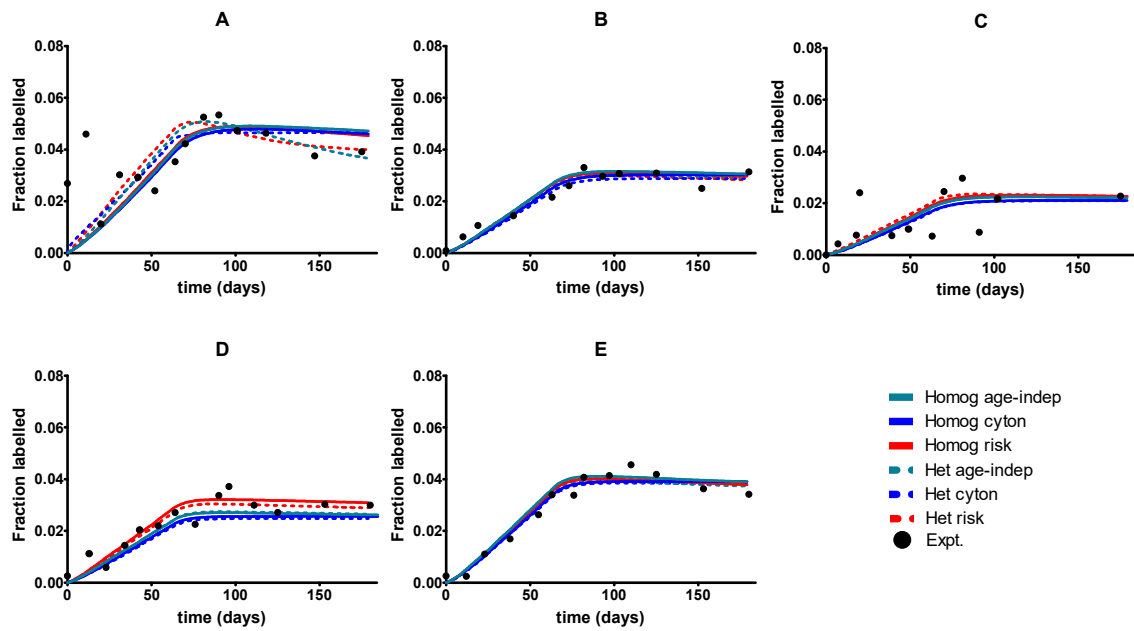
## Memory CD8<sup>+</sup> T cells



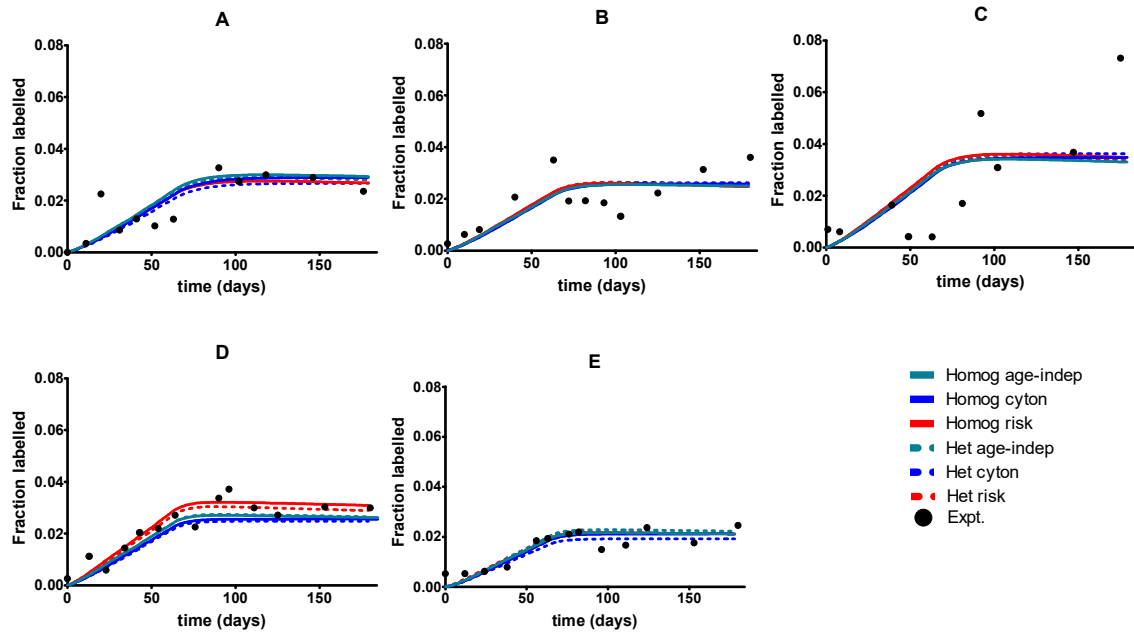
### Supplementary Figure S3. Best fit distributions for memory T cells.

The experimental data from 5 individuals (A-E) from the heavy water study were fitted with the homogeneous and heterogeneous versions of the three paradigms (age-independent, cyton and risk). The best fit censored lifespan distributions (i.e. the distribution of the time from cell birth to either death or division whichever occurs first) are plotted. Top two rows show the best fits for memory CD4<sup>+</sup> T cells and the bottom two rows the best fit for memory CD8<sup>+</sup> T cells. Each coloured curve corresponds to a different individual.

## A. Naive CD4<sup>+</sup> T cells



## B. Naive CD8<sup>+</sup> T cells

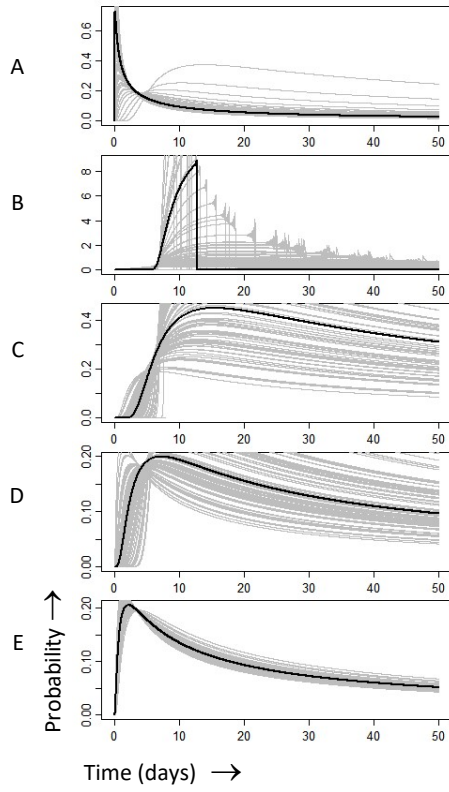


### Supplementary Figure S4. Best fit of the 6 models to Naïve CD4<sup>+</sup> and CD8<sup>+</sup> T cell data.

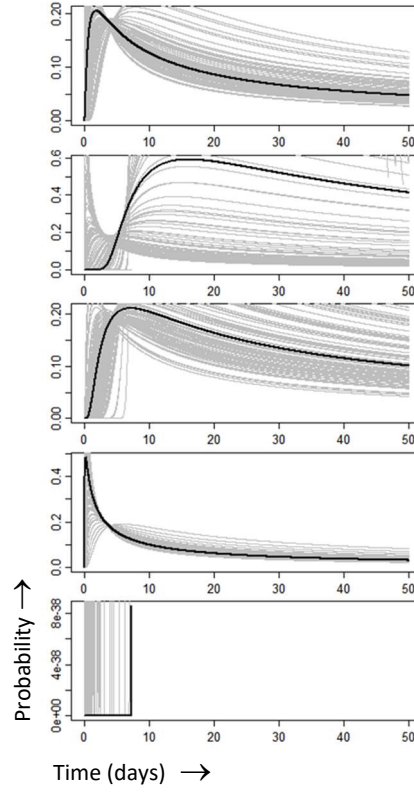
A different subject (A-E) is shown in each panel. Here the cyton and risk models are described using the gamma distribution; similar results are obtained using the lognormal distribution for the cyton model whilst the lognormal version of the risk model provided a very poor fit to the data. Data taken from [33].

### A. Homogenous lognormal

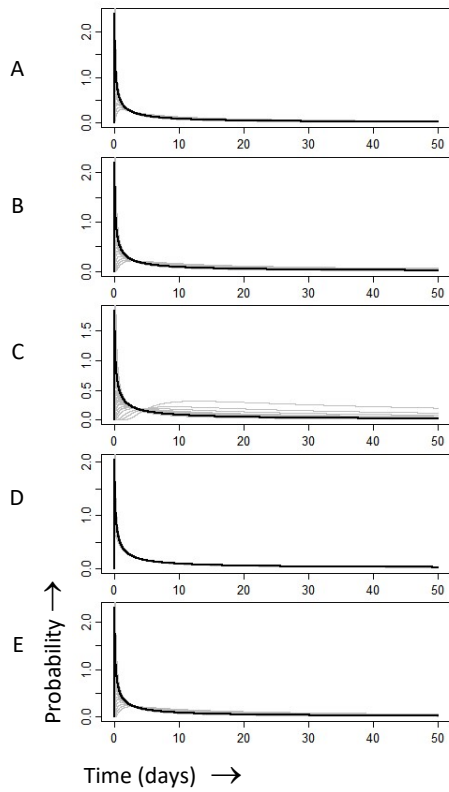
Naïve CD4<sup>+</sup> T cells



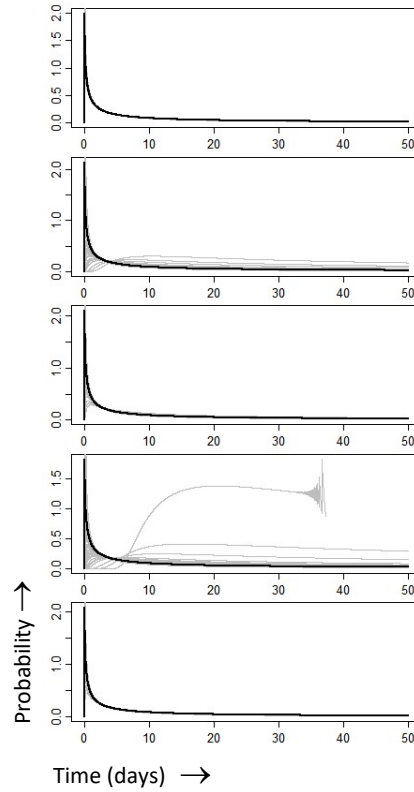
Naïve CD8<sup>+</sup> T cells



Memory CD4<sup>+</sup> T cells

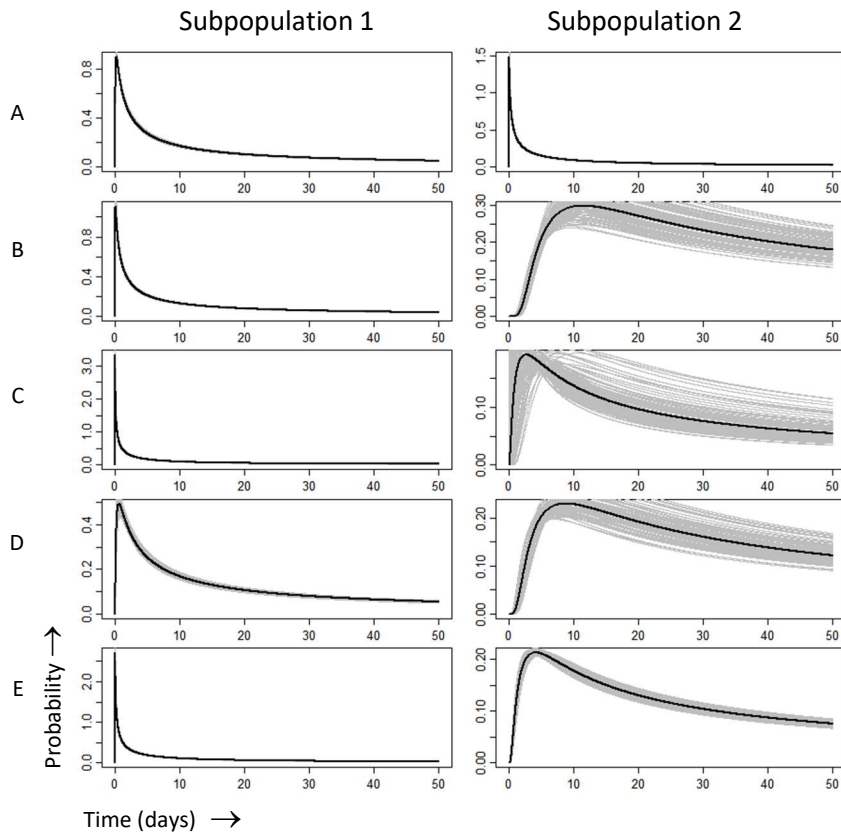


Memory CD8<sup>+</sup> T cells

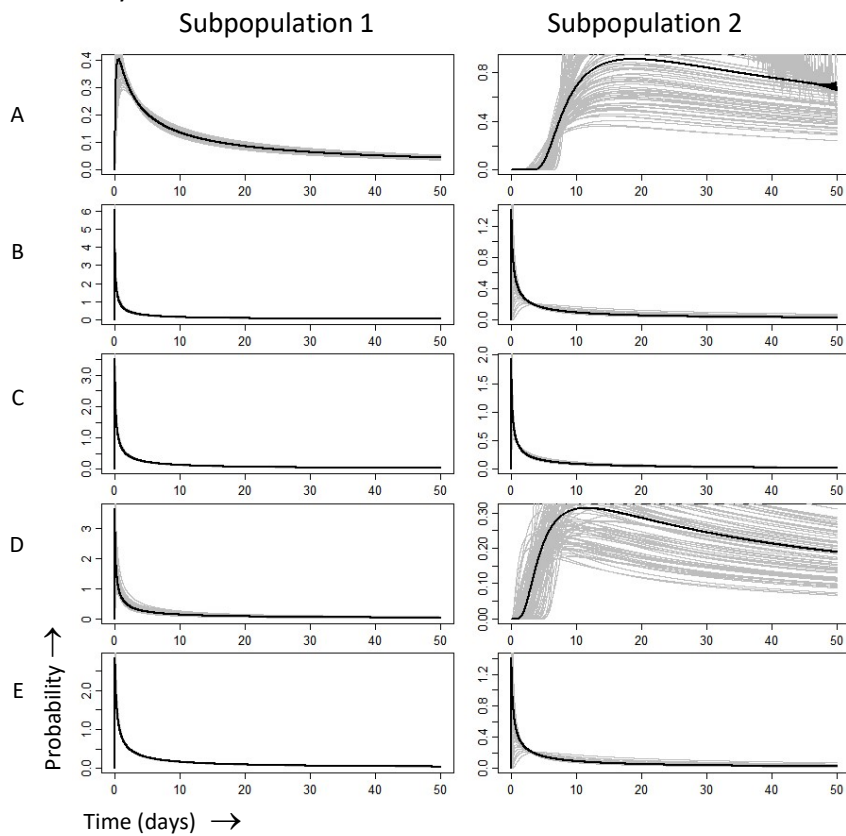


## B. Heterogeneous lognormal

Memory CD4<sup>+</sup> T cells



Memory CD8<sup>+</sup> T cells



### **Supplementary Figure S5. Alternative approach to determining paradigm**

Models based on lognormal distributions in which parameters were free to vary across both risk and cyton paradigms were fitted to the naïve CD4<sup>+</sup>, naïve CD8<sup>+</sup>, memory CD4<sup>+</sup> and memory CD8<sup>+</sup> T cell heavy water labelling data. The best fit distributions were found and the probability of an event conditional on survival to that point plotted. The thicker black line is the probability from the best fit distribution, the grey lines are 100 trajectories created by sampling the parameters from the normal distribution centered on the best fit parameter with standard deviation given by the standard deviation of the parameter estimate.

**A.** Probability distributions resulting from fitting homogenous lognormal model to naïve T cells (top panel) and memory T cells (bottom panel). CD4<sup>+</sup> T cells are shown on left, CD8<sup>+</sup> T cells on right.

**B.** Probability distributions resulting from fitting heterogeneous lognormal model to memory CD4<sup>+</sup> T cells (top panel) and memory CD8<sup>+</sup> T cells (bottom panel). Distribution for the faster subpopulation shown on the left, and for the slower subpopulation on the right.

The lognormal distribution cannot describe the age-independent paradigm so here we can only compare between the risk and cyton paradigms. For naïve T cells the distribution is rather poorly identified. For memory T cells the best fit distributions are strongly supportive of the risk paradigm (heavily left skewed with probability decreasing with age) rather than the cyton paradigm, particularly for the homogeneous model and for the faster of the two subpopulations for the heterogeneous model (the subpopulation that can best be identified from the labelling data).

## Supplementary Tables

		Homogeneous					Heterogeneous				
		Age-indep	Gamma		Lognormal		Age-indep	Gamma		Lognormal	
			Cyton	Risk	Cyton	Risk		Cyton	Risk	Cyton	Risk
Naive CD4 <sup>+</sup> T cells	A	<b>0</b>	3.55	2.53	2.4	20.28	4.81	16.04	16.81	16.47	36.28
	B	<b>0</b>	2.69	0.92	2.72	61.39	4.94	19.26	19.67	19.71	81.56
	C	<b>0</b>	3.55	4.38	3.36	40.44	8.88	26.91	27.6	26.66	64.23
	D	<b>0</b>	2.28	2.88	2.25	63.73	7.12	17.1	18.14	17.17	79.37
	E	<b>0</b>	2.52	1.4	2.21	57.52	5.86	19.72	18.53	18.92	74.97
Naive CD8 <sup>+</sup> T cells	A	<b>0</b>	37.17	37.09	37.11	74.31	42.28	59.64	60.29	60.09	98.01
	B	<b>0</b>	2.96	3.59	2.91	42.5	7.71	22.39	22.92	22.24	62.44
	C	<b>0</b>	12.99	12.94	12.97	27.57	19.25	42.24	42.73	42.82	57.65
	D	<b>0</b>	3.51	2.46	2.75	35.68	3.68	15.22	16.27	15.04	51.49
	E	<b>0</b>	2.03	2.45	2.07	70.2	7.21	18.57	18.99	18.78	87.7

**Supplementary Table S1. Normalised AICc for fits to naïve T cell data.**

Normalised AICcs for the fits of the ABM to 63 day heavy water labelling data in naïve CD4<sup>+</sup> and CD8<sup>+</sup> T cells. Bold font with grey shading denotes the winning model for that data set (i.e. model with the lowest AICc). AICcs are normalised by subtracting the AICc of the winning model (so the winning model has an AICc of zero by definition). The median normalised AICc is plotted in **Figure 2**.

		Homogeneous					Heterogeneous				
		Age-indep	Gamma		Lognormal		Age-indep	Gamma		Lognormal	
			Cyton	Risk	Cyton	Risk		Cyton	Risk	Cyton	Risk
Memory CD4 <sup>+</sup> T cells	A	29.8	35.54	31.85	29.99	21.95	<b>0</b>	18.2	17.42	16.12	16.96
	B	26.89	32.65	29.29	27.36	21.41	<b>0</b>	18.51	17.09	17.37	18.88
	C	0.69	7.2	4.16	3.3	<b>0</b>	2.1	26.61	27.24	27.07	27.5
	D	11.85	16.65	12.99	10.83	10.06	<b>0</b>	12	12.63	11.67	24.94
	E	24.34	30.87	24.84	21.72	10.34	<b>0</b>	12.97	12.38	12.73	13.65
Memory CD8 <sup>+</sup> T cells	A	5.87	12.55	8.82	4.59	<b>0</b>	3.88	22.84	22.65	21.86	22.86
	B	<b>0</b>	6.49	5.49	4.41	2.44	1.38	77.18	77.26	77.32	75.6
	C	8.19	15.48	11.46	6.96	<b>0</b>	1.09	19.96	21.07	20	20.96
	D	<b>0</b>	7.54	6.59	5.35	5.15	6.74	Inf	Inf	Inf	Inf
	E	25.04	30.85	27.59	22.82	15.44	<b>0</b>	16.55	15.76	15.25	13.23

**Supplementary Table S2. Normalised AICc for fits to memory T cell data.**

Normalised AICcs for the fits of the ABM to 63 day heavy water labelling data in memory CD4<sup>+</sup> and CD8<sup>+</sup> T cells. Bold font with grey shading denotes the winning model for that data set (i.e. model with the lowest AICc). Inf denotes infinity (there are too many parameters in the model for the number of data points available). AICcs are normalised by subtracting the AICc of the winning model (so the winning model has an AICc of zero by definition). The median normalised AICc is plotted in **Figure 2**.

Paradigm	Shape	Scale
Age-independent	1	(0.5, 3000)
Risk	(0.6,0.99)	(0.5, 3000)
Cyton	(2,100)	(0.5, 3000)

**Supplementary Table S3. Parameter constraints for model fitting.**

For the gamma distribution there is an exact correspondence between the shape parameter and the underlying paradigm. Therefore, when fitting age-independent, cyton and risk models based on the gamma distribution the parameter constraints tabulated above were used. For the lognormal distribution the correspondence is less precise and so we fitted all models using a single parameter range ((0.5, 3000) ; (0,2.5)) but then discarded parameter combinations giving a modal lifespan >2 days for the risk paradigm and <7 days for the cyton paradigm.

Individual	U
Subject 1	0.2684
Subject 2	0.2936
Subject 3	0.3526
Subject 4	0.2907

**Supplementary Table S4. Parameters of Label Availability.**

Parameters  $f$ ,  $\delta$ ,  $\beta$  which describe label availability in subjects A-E in the heavy water labelling experiment and parameter U which describes label availability in subjects 1-4 in the deuterated glucose labelling experiment were estimated from successive measurements of label availability in plasma in the case of deuterated glucose or urine in the case of heavy water. Parameters for heavy water were, as expected, identical to those previously reported for the same data set [33] and so are not repeated here, parameters for deuterated glucose are reported above.